frontiers | Frontiers in Earth Science

TYPE Original Research
PUBLISHED 15 November 2024
DOI 10.3389/feart.2024.1487176

OPEN ACCESS

EDITED BY
Yong Wang,
Southwest Petroleum University, China

REVIEWED BY
Xiaodong Deng,
China University of Geosciences
Wuhan, China
Wei Wang,
China University of Geosciences
Wuhan, China

*CORRESPONDENCE
Lin Li,
clark.li@cugb.edu.cn

RECEIVED 27 August 2024
ACCEPTED 29 October 2024
PUBLISHED 15 November 2024

CITATION
Wei Q, Li L, Li S-R, Santosh M, Alam M, Chen Z-Y, Li M-G, Chen X-D, Wen Z-H and Liu J-W (2024) Titanite as an indicator of granite fertility and gold mineralization in the Xiaoqinling gold province, North China Craton.
Front. Earth Sci. 12:1487176.
doi: 10.3389/feart.2024.1487176

Titanite as an indicator of granite fertility and gold mineralization in the Xiaoqinling gold province, North China Craton

Quan Wei [1,2,3], Lin Li [1,4]*, Sheng-Rong Li[1,2], M. Santosh [2,5], Masroor Alam [6], Zhen-Yu Chen [3], Min-Gang Li[1,2], Xiao-Dan Chen [3], Zi-Hao Wen [1,2] and Jia-Wei Liu[1,2]

[1]State Key Laboratory of Geological Processes and Mineral Resources, China University of Geosciences, Beijing, China, [2]School of Earth Science and Resources, China University of Geosciences, Beijing, China, [3]MNR Key Laboratory of Metallogeny and Mineral Assessment, Institute of Mineral Resources, Chinese Academy of Geological Sciences, Beijing, China, [4]Institute of Earth Sciences, China University of Geosciences, Beijing, China, [5]Department of Earth Sciences, University of Adelaide, Adelaide, SA, Australia, [6]Department of Earth Sciences, Karakoram International University, Gilgit, Pakistan

The Xiaoqinling gold province, located in the southern margin of the North China Craton (NCC), is the second largest gold-enriched region in China. In this region, the Mesozoic Huashan (HS) and Wenyu (WY) plutons are the major magmatic intrusions coeval with gold mineralization, although they show contrasting characteristics in the distribution of gold. In this study, we use geochemical features of titanite determined by LA-ICP-MS and EPMA analyses and elemental mapping to decipher the mechanisms that led to the difference in gold enrichment related to the two plutons. Titanite from the Wenyu granitic pluton exhibits significantly higher $(La/Sm)_N$, $(La/Yb)_N$, ΣLREE/ΣHREE ratios, and ΣREE concentration and slightly higher $(Gd/Yb)_N$ values than those of the Huashan Pluton, suggesting that the Wenyu pluton might have experienced more complex magmatic evolution, widespread hydrothermal alteration, and higher silica activity in the melt than the Huashan pluton. The titanite grains from the Huashan pluton show higher $(Nb/Ta)_N$ and $(Lu/Hf)_N$ values and significantly lower Zr concentration than those of the Wenyu pluton. The titanite grains from the Wenyu pluton show higher vanadium and gallium concentrations and Fe/Al ratio than those of the Huashan pluton, indicating comparatively higher fo_2. Furthermore, the titanite grains from Wenyu pluton indicate higher water content in the magma. In addition, magma mingling and magmatic hydrothermal fluids derived from the crust/mantle are critical sources for ore-forming materials. These results suggest that the Wenyu pluton is more conducive to gold migration and enrichment than the Huashan pluton.

KEYWORDS

titanite, LA-ICP-MS, Huashan and Wenyu granitic plutons, gold fertility, Xiaoqinling gold province

1 Introduction

Titanite ($CaTiSiO_5$) is a common and widespread accessory mineral in igneous and metamorphic rocks (Gribble and Hall, 1993; Klein and Dutrow, 2007; Perkins, 2013), and it is an important host for rare-earth elements (REEs), high-field-strength elements (HFSEs), etc., with its slow diffusion and high closure temperature making it an important mineral to trace magma history (Buick et al., 2007; Cherniak, 2006; Chiaradia et al., 2013; Frost et al., 2001; Hayden et al., 2008; Holder et al., 2019; Ismail et al., 2014; Kohn, 2017; Lucassen et al., 2011; McLeod, 2009; McLeod et al., 2010; Piccoli et al., 2000; Prowatke and Klemme, 2005; Smith et al., 2009; Tiepolo et al., 2002; Xu et al., 2015). Several previous studies reported that titanite geochemistry could indicate the physicochemical conditions of evolving magmatic systems (Frost et al., 2001; McLeod et al., 2010; Piccoli et al., 2000; Gromet and Silver, 1983; King et al., 2013; Kowallis et al., 1997; Nakada, 1991; Wones, 1989; Kowallis et al., 2018), and the mineral has been considered an indicator for some of the important mineral deposits such as W(Cu) skarn, Cu–U–Au–Ag, Mo, and Cu–Mo–Au deposits (Xu et al., 2015; Aleksandrov and Troneva, 2007; Che et al., 2013; Kontonikas-Charos et al., 2019; Pan et al., 2018; Song et al., 2019; Wang et al., 2011; Wang et al., 2013; Xie et al., 2009; Xie et al., 2010). Magma fertility implies that magmas with certain chemical signatures may be predisposed to form Au mineralization. Magma fertility, especially metal magma fertility, has been widely used to evaluate the metallogenic potential of Au, Cu, other essential minerals, and related magmatism in recent years (Chen et al., 2019; Grondahl and Zajacz, 2022; Nathwani et al., 2022; Redin et al., 2022; Shu et al., 2019).

Magmatism with high potential for metal fertility in large-scale metallogenesis is usually associated with specific tectonic environments (Li et al., 2022; Li et al., 2016; Li et al., 2015; Li and Santosh, 2014; Li and Santosh, 2017; Santosh and Groves, 2022), substantial metallogenic components, sustained energy systems, and adequate channels for transportation and favorable sites for accumulation (Mao et al., 1999). The Xiaoqinling metallogenic region is the second largest gold-producing area in China (second only to Jiaodong), and it is considered a typical representative of gold deposits formed through decratonization (Zhu et al., 2015; Zhu et al., 2012). As the main type of gold deposit in this area, the quartz vein-type gold deposits formed in the extensional tectonic setting and the associated large-scale magmatism are dated as ca. 130 Ma (Li and Santosh, 2014; Li and Santosh, 2017; Zhu et al., 2015; Li et al., 2014; Li et al., 2013). In the Xiaoqinling area, the Wenyu (WY) and Huashan (HS) intrusions are two major Mesozoic plutons with similar ages and mostly coeval with gold mineralization. By comparing the Mesozoic plutons with typical gold metallogenic quartz vein features of fluid inclusion microthermometry and H, O, C, S, and Pb isotopes of the gold deposits, previous researchers suggested that these Au deposits are temporally and spatially associated with the Mesozoic granites in this area (Chen, 2006; Fan et al., 2000; Feng et al., 2009; Jian, 2010; Wang et al., 2022; Wang et al., 1994; Wu, 2016; Xie et al., 1998; Zhao et al., 2018; Zhou et al., 2011). Xu et al. (1997) reported that the Wenyu pluton is favorable to the formation, cycle, and deposition of ore-bearing fluids. Xie et al. (1998) reported that the gold metallogenic quartz vein fluid inclusion feature is similar to that of the Wenyu pluton, while it is quite different from that of the Huashan pluton. The Wenyu pluton has a genetic correlation with Xiaoqinling area gold mineralization (Wang et al., 1994; Xie et al., 1998; Liu et al., 2022; Qi, 2010; Wen et al., 2020; Zhi et al., 2019). Centering on the Wenyu pluton, the gold metallogenic quartz vein fluid inclusion homogenization temperature shows a decreasing trend. The Wenyu pluton plays an important role in controlling the spatial distribution of gold deposits and the metallogenic temperature, and it provides thermodynamic conditions (Qi, 2010; Li et al., 1996). Ore metals might be sourced from the Taihua group, and gold mineralization is closely related to Wenyu pluton in the Xiaoqinling area (Liu et al., 2022; Qi, 2010; Wen et al., 2020; Zhi et al., 2019; Li et al., 1996; Li et al., 2012a; Wu, 2019; Zhao et al., 2011; Zhou et al., 2015; Zhou et al., 2014). Yang and Santosh (2020) reported the critical contribution of Mesozoic magmatism producing Au deposits in the convergent margins of NCC. The Huashan and Wenyu plutons were formed by multistage magmatism between 141.0 ± 1.6 and 127.7 ± 0.6 Ma (Guo et al., 2009; Li et al., 2012b; Mao et al., 2010; Zhao et al., 2012), overlapping the ages of major gold deposits. This temporal consistency indicates a possible correlation between gold mineralization and granitoid magmatism in the area (Li et al., 2012b). With the similar geotectonic background and mineralization age, there are significantly more gold deposits around the Wenyu pluton than Huashan pluton (Figure 1), which might indicate the varying fertility of magmas of the both plutons in terms of Au.

This study presents the detailed chemical composition of titanite from the Huashan and Wenyu plutons, including the concentration of REEs, gallium, and vanadium, as well as the Fe/Al ratios to characterize the physicochemical conditions, including magma composition, fo_2, and water contents in both granitic plutons. Based on the results, we evaluate the granite fertility and discuss the role of magmatism during gold mineralization; we also discuss the mechanisms responsible for the difference in the spatial distribution of the gold deposits around the Huashan and Wenyu plutons. Our study has important implications for characterizing more fertile magmas using titanite mineral and setting guidelines for prospecting and exploration of gold deposits related to granitic magmatism globally.

2 Geological setting and gold deposit characteristics

2.1 Geological setting

The Xiaoqinling gold metallogenic area is located on the southern margin of the NCC and the northern boundary of the Qinling Orogenic Belt (Figure 1A). The collision between the southern part of the NCC and the Yangtze Block forming the Qinling–Dabie orogenic belt triggered the Triassic deformation that affected the southern domain of the NCC (Dong and Santosh, 2016; Dong et al., 2021; Dong et al., 2011; Wu et al., 2006; Zhang et al., 2001). The westward subduction of the Paleo-Pacific Plate caused extensive tectonic activity in the eastern NCC in the early Cretaceous (Zhu et al., 2015; Zhu et al., 2012). In the study area (Figure 1B), the tectonic framework is dominated by the two reginal faults, i.e., the Xiaohe and the Taiyao faults in the north and south, respectively, with two local faults, the Huanchiyu and

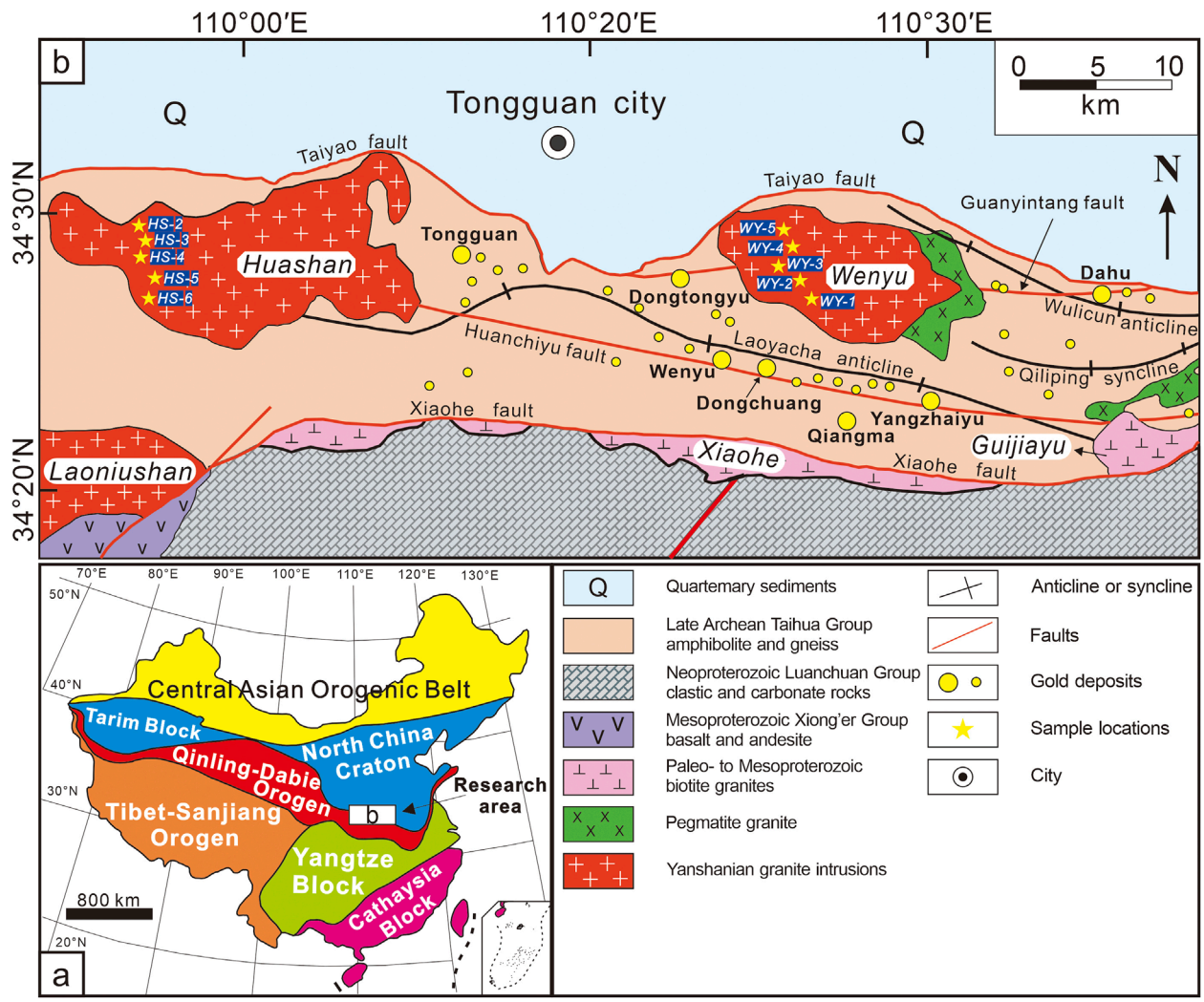

FIGURE 1
Geological map of the Xiaoqinling area. **(A)** The box indicated by the arrow denotes the location of research area. **(B)** Geological map mainly showing the distribution of basement rocks, main structures, and the spatial difference of gold deposits around the Huashan and Wenyu plutons in the Xiaoqinling area NCC. Modified from Li et al. (1996).

Guanyintang faults (Zhao et al., 2012; Deng et al., 2016). From the north to the south, several major fold structures such as the Wulicun anticline, Qishuping syncline, and Laoyacha anticline occur in the region, which mainly trend in the east–west direction (Luan et al., 1985). The basement rocks belong to the Neoarchean Taihua group and are mainly composed of amphibolites and gneisses, together with basalt and andesites of the Middle Paleozoic Xiong'er group, and the clastic rocks and carbonate rocks of the Neoproterozoic Luanchuan group. Multiple magmatic intrusions are recognized in this area. Proterozoic magmatism mainly includes Xiaohe biotite granite, Guijiayu biotite–hornblende granite, and widely distributed pegmatites. The Yanshanian period biotite monzonitic granites mainly include Laoniushan, Huashan, and Wenyu plutons, covering areas of 440 km^2, 130 km^2, and 71 km^2, respectively (Wen et al., 2020; Wang et al., 2012). The Wenyu pluton shows more clear characteristics of the involvement of mantle-derived material in the magma source (Wen et al., 2020; Zhi et al., 2019).

2.2 Gold deposit characteristics

In the Xiaoqinling area, the known gold deposits are mostly distributed around Mesozoic granitoids and emplaced within the Proterozoic metamorphic basement rocks. These gold deposits primarily occur within quartz veins, showing limited occurrence in altered rocks (Zhu et al., 2015). Compared with the Huashan pluton, the Wenyu pluton is surrounded by more gold deposits (Figure 1B). The Wenyu pluton is surrounded by some large gold deposits such as Dongtongyu, Wenyu, Dongchuang, Qiangma, Yangzhaiyu, and Dahu and numerous smaller gold deposits. However, there are few gold deposits around the Huashan Pluton, such as the Tongguan deposit.

The gold in these deposits is predominantly native gold and electrum, which is extracted as inclusions or veinlets in pyrite and some in quartz, coexisting with galena and chalcopyrite (Zhou et al., 2014). The main mineralized alterations in these

deposits include silicification, sericitization, pyritization, and K-feldspathization, and the mineralization process is generally divided into four stages: initial quartz–pyrite stage, second quartz–pyrite stage, quartz–base metal sulfide stage, and final carbonate-dominantstage (Mao et al., 2002).

3 Petrography and samples

The locations of fresh biotite monzogranite sample are shown in Figure 1B. Titanite grains were separated from the samples using standard heavy-liquid and magnetic methods, followed by handpicking under a microscope. The titanite grains were mounted in epoxy, polished to expose the surface, and examined using BSE images to select suitable targets for *in situ* analysis. The selected domains are mostly the center of the grains to minimize the effect of the subsolidus exchange reaction between titanite and the surrounding minerals.

The Wenyu pluton is roughly elliptical with an exposed area of approximately 71 km^2 and can be divided into the marginal, transitional, and upper facies. The marginal facies consist primarily of fine- to medium-grained biotite monzogranite. The transitional facies are predominantly constituted by grayish–white medium-grained biotite monzogranite, which is the largest outcrop facies of the Wenyu pluton. The lithology of the upper facies is gray–white fine-grained biotite monzonitic granite (Wang et al., 2010; Yu et al., 2013). The Wenyu samples were medium-grained biotite monzogranite and collected from transitional facies.

The Huashan pluton shows east–west extension, with an exposed length of approximately 21 km and width of 6.6 km, covering an area of 130 km^2. Based on lithology, the Huashan pluton can be divided into three facies from the west to the east. The middle part is mainly constituted by fine- to medium-grained amphibole monzogranite, and the flanks consist predominantly of medium-grained biotite monzogranite (Zhang et al., 2015). The Huashan samples were medium-grained biotite monzogranite and collected from the western flank.

The Wenyu and Huashan plutons are biotite monzogranites with a similar mineral assemblage. Mineralogically, the samples were composed mainly of plagioclase (30%–35%), K-feldspar (30%–35%), quartz (20%–25%), and biotite (2%–5%). The accessory minerals mainly include zircon, apatite, magnetite, and titanite (Figure 2). Titanite grains, under cross-polarized light, are mainly yellow/brown in color and appear homogeneous (Figures 2C, D). Titanite grains vary in size between 100 and 350 μm and occur mostly as euhedral to subhedral wedge-shaped grains and partially as crystallographic twins (Figure 2D), which are adjacent to, or included in, biotite, magnetite, K-feldspar, plagioclase, and quartz (Figures 2C–H). Zircon and magnetite were also observed in the interior of titanite grains (Figures 2E, H).

4 Analytical methods

Trace element analysis of titanite was conducted by LA-ICP-MS at the Wuhan Sample Solution Analytical Technology Co., Ltd., Wuhan, China. Detailed operating conditions for the laser ablation system and the ICP-MS instrument and data reduction are the same as described by Zong et al. (2017). Laser sampling was performed using a GeoLasPro laser ablation system equipped with a COMPexPro 102 ArF excimer laser (wavelength of 193 nm and maximum energy of 200 mJ) and a MicroLas optical system. An Agilent 7700e ICP-MS instrument was used to acquire ion-signal intensities. Helium was applied as a carrier gas. Argon was used as the make-up gas and mixed with the carrier gas via a T-connector before entering the ICP. A "wire" signal smoothing device was included in this laser ablation system (Hu et al., 2015). The spot size, frequency, and energy of the laser were set to 44 μm, 5 Hz, and 80 mJ, respectively. Trace element compositions of minerals were calibrated against various reference materials (NIST610, BHVO-2G, BCR-2G, and BIR-2G) without using an internal standard (Liu et al., 2008). Each analysis incorporated a background acquisition of approximately 20–30 s followed by 50 s of data acquisition from the sample. An Excel-based software ICPMSDataCal was used to perform off-line selection and integration of background and analyzed signals, time-drift correction, and quantitative calibration for trace element analyses (Liu et al., 2008).

A JEOL JXA-8230 Electron Probe Micro Analyzer (EPMA) housed at the MLR Key Laboratory of Metallogeny and Mineral Assessment, Institute of Mineral Resources, Chinese Academy of Geological Sciences, was used for elemental analysis and mapping of titanite. The analytical conditions are 15 kV accelerating voltage, 20 nA beam current, and 5 μm beam diameter. The calibrations and detection limits are shown in Supplementary Table 1. Element mapping conditions are 15 kV accelerating voltage, 30 nA beam current, dwell time of 100 millisecond, and spot model.

5 Results

5.1 EPMA data with compositional mapping

The backscattered electron (BSE) images of the representative titanite grains from the two plutons are presented in Figure 3. The major elemental compositions of titanite from the Huashan (319 data points) and Wenyu (329 data points) plutons are given in Supplementary Tables 2, 3, respectively. The structural formulae of titanite were calculated (based on Si=1) according to the procedure described by Oberti et al. (1991), assuming full occupancy of the Ca, Si, and Ti sites and calculating all Fe as Fe^{3+} values. The OH^- and O^{2-} are also calculated based on the same procedure. The analytical elements of the a.p.f.u. variation range and mean value are shown in Supplementary Table 4.

The EPMA elemental maps (Figure 4) of the typical titanite grain from the Wenyu pluton (Figure 3A) display the distribution of the major element Ca and trace elements Al and Y in the elemental maps. The relatively brighter zone in the BSE image (Figure 3A) corresponds to the lower-Ca, lower-Al, and higher-Y regions in the EPMA elemental maps. There is no obvious relationship between BSE image zones and the distribution of Ti, Si, V, Cl, Dy, Sn, F, Fe, Mn, and uranium content in the EPMA elemental maps, although relatively higher Nb and Ta is observed as the higher-Nb area displays a beaded-like appearance. All the mapped elements of the titanite grain from the Wenyu pluton display a sharp boundary, except for U.

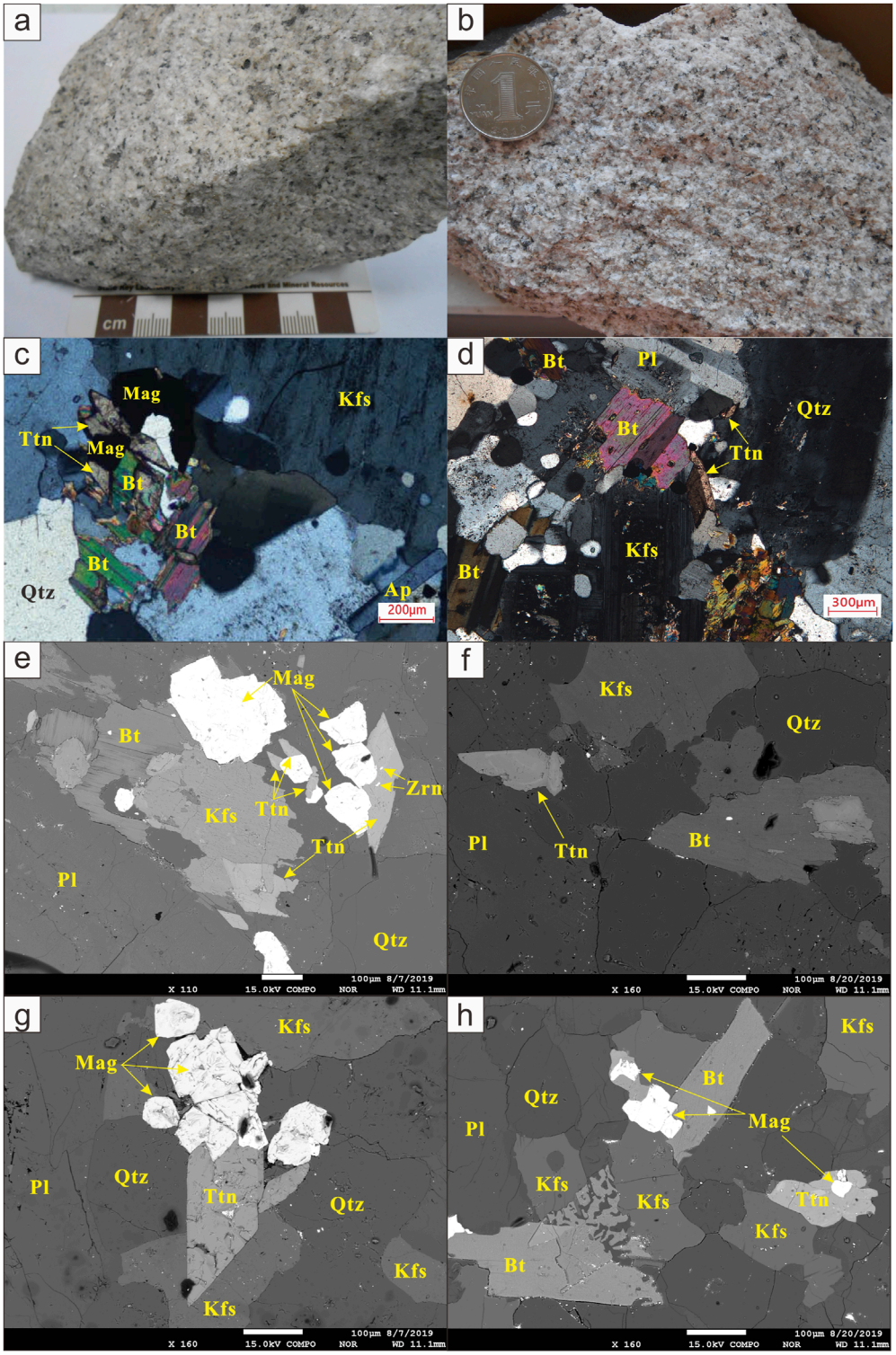

FIGURE 2
Typical biotite monzogranite hand specimen photo from the Wenyu **(A)** and Huashan plutons **(B)**. Typical photomicrographs (under the cross-polarized light condition) of the Wenyu **(C)** and Huashan plutons **(D)**. Typical BSE images from the Wenyu **(E, G)** and Huashan plutons **(F, H)**. Mineral assemblages include plagioclase (Pl), K-feldspar (Kfs), quartz (Qtz), biotite (Bt), magnetite (Mag), apatite (Ap), and titanite (Ttn).

The EPMA elemental maps (Figure 5) of the typical titanite grain from the Huashan pluton (Figure 3B) show that there is a lack of a distinct distribution relationship among the major elements Si and Ca and the trace elements V, Y, Sn, Ta, and Cl with the zones (bright zones) on the BSE image of the titanite grain, but there are relatively low-Ti and high-Ti zones. The distribution of some trace elements

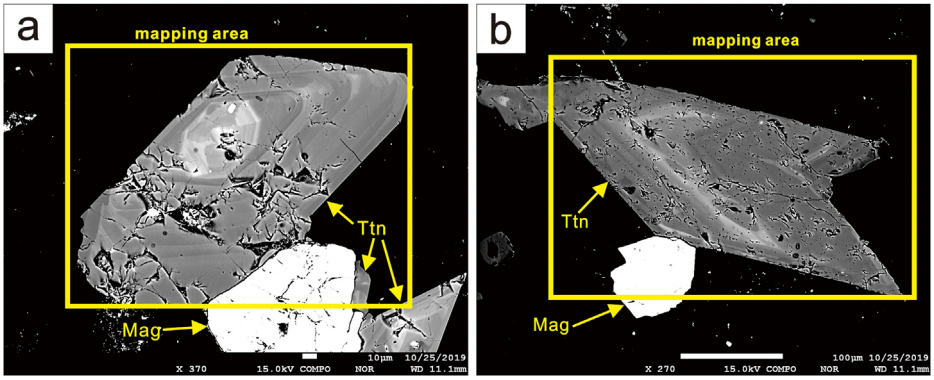

FIGURE 3
Typical titanite grain BSE images from the Huashan and Wenyu plutons. **(A)** Wenyu pluton titanite grain showing oscillatory zones. **(B)** Huashan pluton titanite grain.

varies between the two zones. The high-Ti zone corresponds to the relatively higher Nb, U, Mn, Al, and Fe and slightly lower Dy and F. In addition, there is relatively higher Nb and U distribution in the brighter region of the BSE image (Figure 3B). All the mapped elements of the titanite grain from the Huashan pluton display a sharp boundary.

5.2 Titanite trace elements

The titanite LA-ICP-MS trace element data are given in Supplementary Table 5. The ΣREE concentration in titanite from the Wenyu pluton is much higher than those of the Huashan pluton. In the Huashan pluton, the ΣREE content in titanite ranges from 2,016.87 ppm to 10,769.98 ppm (average 4,758.30 ppm), while the ΣLREE/ΣHREE ratio ranges from 0.61 to 8.24 (average 2.49). The titanite grains from the Huashan pluton show depleted LREE, flat HREE patterns, and wider range of HREE content than those of the Wenyu pluton. In addition, the titanite samples from the Huashan pluton display a wide range of Eu anomalies (as their δEu values range from 0.22 to 1.42, average being 0.80, but record one abnormal value of 3.73, which was excluded for the calculation of the mean value). The δCe values vary from 0.45 to 0.70, with a mean of 0.60. On chondrite-normalized REE diagrams, the titanite grains from the Huashan pluton have $(La/Sm)_N$ ratios from 0.05 to 0.58 (average 0.26), $(La/Yb)_N$ ratios from 0.06 to 3.95 (average 0.90), and $(Gd/Yb)_N$ ratios from 0.63 to 5.34 (average 2.15). The ratios of $(Nb/Ta)_N$ range from 0.45 to 4.72, with an average of 1.22. The concentrations of Hf and Lu are 1.26–47.53 (average 18.99) and 3.442–128.69 (average 29.50) ppm, respectively, with $(Lu/Hf)_N$ ratios ranging from 1.20 to 68.81 (average 12.27). The concentrations of Zr range from 33.27 ppm to 702.60 ppm, with a mean of 173.51 ppm.

In the Wenyu pluton, the ΣREE in titanite is in between 3,586.88 ppm and 15,653.24 ppm, with an average of 7,761.60 ppm. The ΣLREE/ΣHREE ratios are from 1.50 to 7.96 (average 4.44). The titanite grains from the Wenyu pluton show depleted HREE and enriched LREE. On chondrite-normalized REE diagrams, Wenyu titanite grains display negative Eu anomalies (δEu values range from 0.36 to 0.89, average 0.57). The δCe values are from 0.61 to 0.74 (average 0.67). The $(La/Sm)_N$, $(La/Yb)_N$, and $(Gd/Yb)_N$ ratios range from 0.26 to 1.19, 0.23 to 6.99, and 0.69 to 5.39, with the averages of 0.57, 2.25, and 2.27, respectively. The ratios of $(Nb/Ta)_N$ range from 0.43 to 1.53 (average 0.91). The concentrations of Hf and Lu are 19.70–370.92 and 13.86–90.05, with the mean of 49.24 and 28.77 ppm, respectively, with $(Lu/Hf)_N$ ratios of 0.87–8.72 (average 4.26). The concentrations of Zr range from 141.22 to 1,623.13 (average 437.92) ppm.

6 Discussion

6.1 Magmatic evolution and titanite genesis

Kowallis et al. (1997), Kowallis et al. (2018) reported that the atomic ratio of Fe/Al in titanite from both volcanic and plutonic rocks is typically close to 1:1 and almost always >1:2. The Fe/Al data range from 0.5 to 1 for the plutonic titanite, which falls roughly in the green area in Figure 6. The possibility of volcanic origin can be ruled out based on the lithological properties of our sample. However, Kowallis (2018) also reported that titanite from metamorphic, hydrothermal, and pegmatitic environments scatter widely in Fe/Al. As shown in Figure 6, the Fe/Al ratio of Wenyu titanite is more concentrated in the plutonic region than that of Huashan. In detail, the Fe/Al data for titanite from the Wenyu pluton, which is in the range of 0.5–1, contributes 86.6% of the total data, while this is only 35.7% for the Huashan pluton. In the Huashan pluton, Fe (average a.p.f.u 0.053) in titanite is slightly lower than Fe (average a.p.f.u 0.054) in titanite from the Wenyu pluton; however, in the Huashan pluton, the Al (average a.p.f.u 0.141) in titanite is much higher than that in titanite from the Wenyu pluton (Al average a.p.f.u 0.141). Based on the whole-rock major elements, Qing and Han (2001) found that the Wenyu pluton shows a relatively lower A/CNK ratio than the Huashan pluton. We suspect that the relatively aluminum-poor titanite in the Wenyu pluton compared to that in the Huashan pluton may reflect a difference in the magmatic composition.

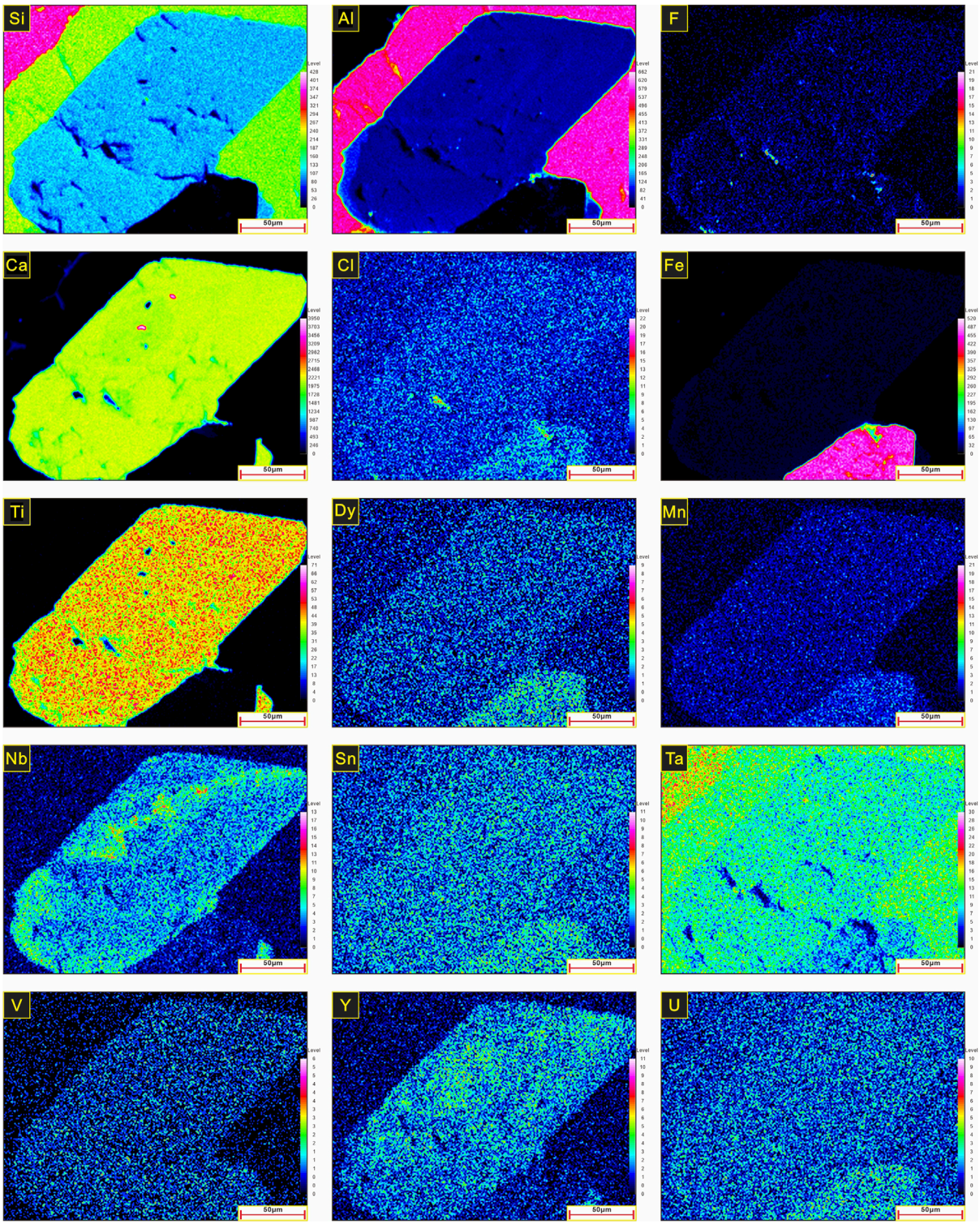

FIGURE 4
EPMA element map of a typical titanite grain from the Wenyu pluton in the Figure 3A mapping area.

Titanite characterized by enrichment in LREE is usually formed during the late magmatic stage (Xiao et al., 2021). Piccoli et al. (2000) reported that the complex zoning in the titanite from the granitic rocks is interpreted to have primarily developed as a result of magmatic processes, and it is strongly controlled by the LREE. In our research, compared with Huashan titanite (Figure 3B), Wenyu titanite (Figure 3A) shows obviously stronger zoning. In Figure 7, the Wenyu pluton shows enriched LREE and depleted

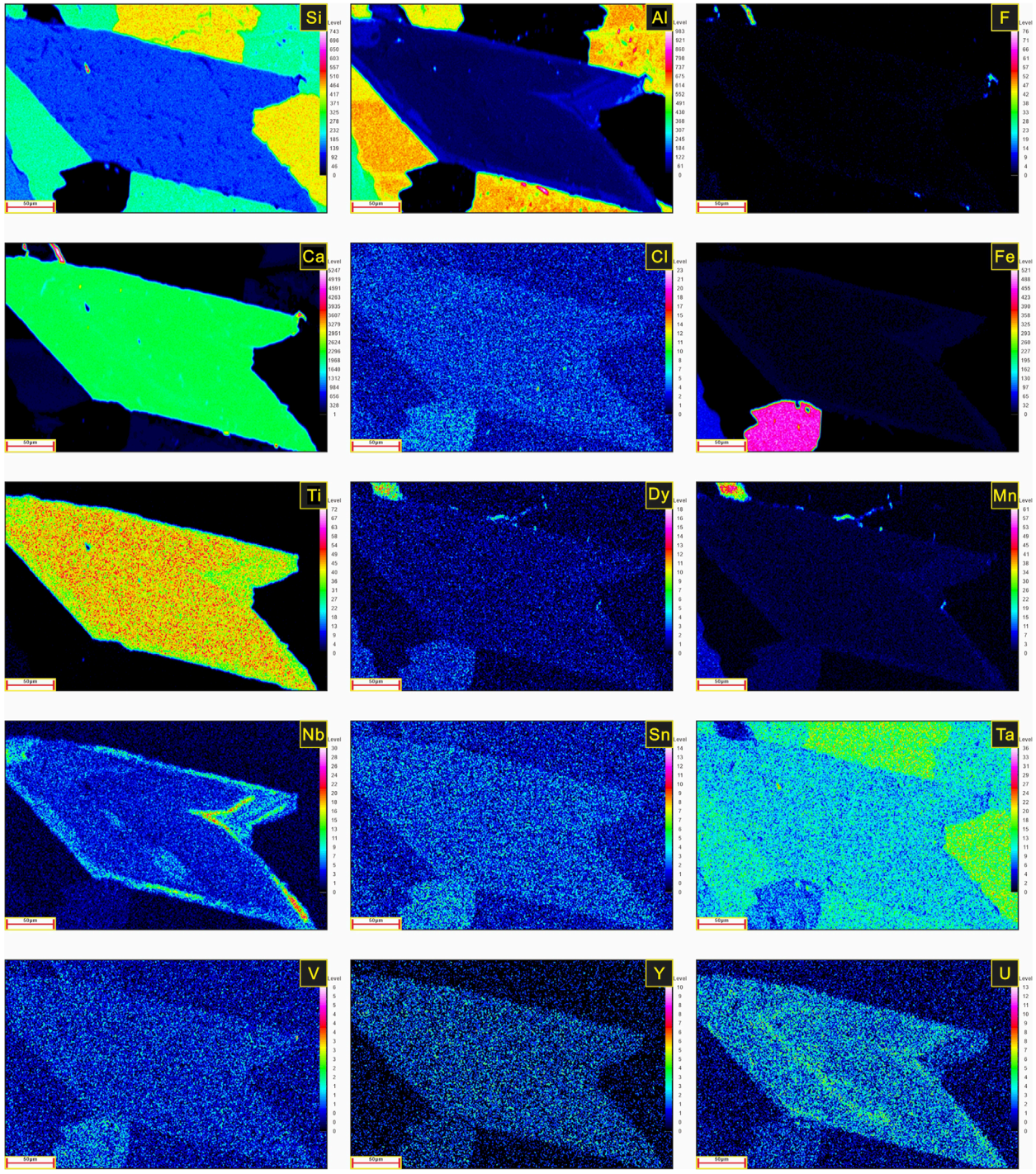

FIGURE 5
EPMA elements map of a typical titanite grain from the Huashan pluton in the Figure 3B mapping area.

HREE patterns. With the variation in the Yb_N content, light and heavy REE fractionation in the Wenyu pluton shows a more marked general evolutionary trend than in the Huashan pluton (Figure 8C). The LREE fractionation in the Wenyu pluton is more obvious than that of the Huashan pluton (Figure 8B). Furthermore, both plutons exhibit similar heavy REE fractionation (Figure 8A), although the Wenyu pluton is more enriched in Yb_N content. In the Huashan pluton, the fractionation of LREE/HREE is not obvious.

Qi, (2010), Qing and Han (2001) compared the whole-rock trace elements of the Wenyu and Huashan plutons and found that the ΣREE and LREE/HREE fractionation is higher in the Wenyu pluton, which shows a similar REE pattern with our titanite result. This is because the Wenyu pluton has higher silica activity

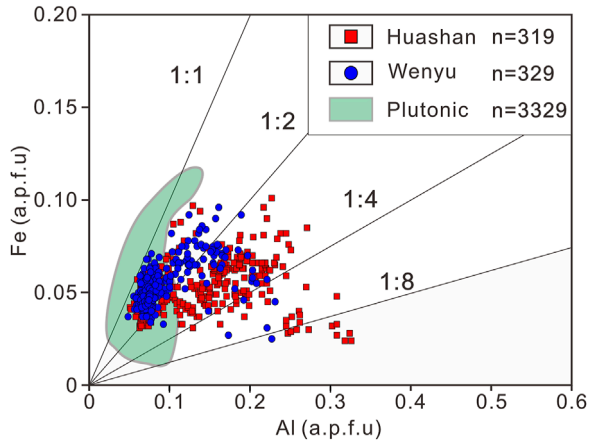

FIGURE 6
The Fe–Al (a.p.f.u.) graph of titanite grains. The "plutonic" region is modified from Kowallis et al. (2018).

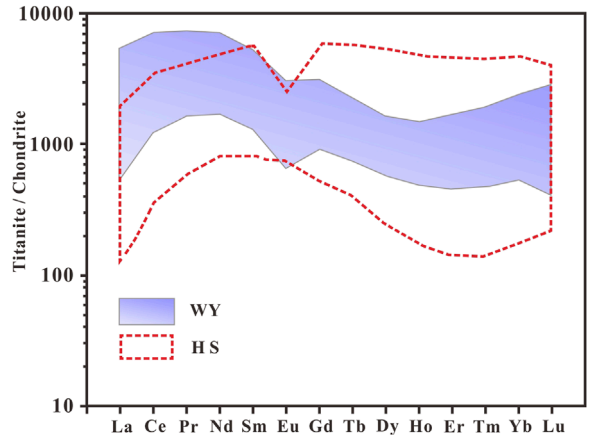

FIGURE 7
Chondrite-normalized fractionation patterns for REE in titanite from the Huashan and Wenyu plutons, normalizing values taken from Boynton (1984) (Zhang, 2015). Shaded areas represent the range from the maximum to minimum values.

in the melt than the Huashan pluton during titanite formation as higher SiO_2 activity facilitates the $LREE^{3+}$ substitution into Ca-site (Kowallis et al., 1997; Qing and Han, 2001) and, during magmatic evolution, including multi-stage magma activities, titanite formed in late magmatic stage, which contributed to the obvious differentiation of LREE and HREE (Qing and Han, 2001; Xiao et al., 2021). In addition, the fo_2 of the Wenyu pluton is higher than that of the Huashan pluton (which will be discussed in Section 6.2 below.), and leaching of the post-magmatic hydrothermal fluids and remobilization of REE might have occurred (Pan et al., 1993). In addition, in previous studies, the zircon U–Pb ages (Huashan: 144 ± 0.6 Ma, Wenyu: 141.4 ± 0.6 Ma to 129.6 ± 0.5 Ma) (Wen et al., 2020) and the pyrite and quartz rhythmic zones (Li et al., 2022) also confirm multi-stage magmatism for the formation of titanite in the Wenyu pluton, which together caused higher fractionation of LREE/HREE in the Wenyu pluton than in the Huashan pluton. Therefore, we argue that titanite from the Wenyu pluton might have experienced a more complex magmatic evolution history, more widespread hydrothermal alteration, and was formed under higher silica activity than titanite from the Huashan pluton.

6.2 Oxygen fugacity

6.2.1 δCe, δEu, and ΣREE

Piccoli et al. (2000) reported that the depletion in REEs may be due to the lower activity of Fe^{3+}, which is needed to compensate for the charge balance of REEs in the titanite structure, which means lowering of oxygen fugacity can diminish the activity of the $(REE^{3+}/Fe^{3+}) \rightleftharpoons (Ca^{2+}, Ti^{4+})$ exchange. In the Wenyu pluton, the ΣREE in titanite ranges from 3,586.88 ppm to 15,653.24 ppm (average 7,761.60 ppm). In the Huashan pluton, the ΣREE in titanite ranges from 2,016.87 ppm to 10,769.98 ppm (average 4,758.30 ppm). Qing and Han (2001) calculated the Fe_2O_3/FeO ratio and $Fe_2O_3/(Fe_2O_3+FeO)$ ratio based on the whole-rock major elements of the Wenyu and Huashan plutons and found that the proportion of Fe^{3+} in the Wenyu pluton is significantly higher than that in the Huashan pluton. Combined with the above evidence, we assume that the titanite sample with higher ΣREE content might have formed in a higher oxidizing crystallization environment, which might imply the higher fo_2 of the Wenyu pluton than the Huashan pluton.

Unlike other REE^{3+}, Eu and Ce are common elements, especially in zircon, which can be used to measure the fo_2 (Wen et al., 2020; Ballard et al., 2002; Trail et al., 2011; Trail et al., 2012) due to their variable valency (Ce: +3, +4; Eu: +2, +3). Previous studies reported that the ionic radii of $^{VII}Ce^{3+}$ (1.07 Å) and $^{VII}Ca^{2+}$ (1.06 Å) are similar (Shannon, 1976). For Ce^{3+}, the Ca-site might be the most favorable substitution site in titanite based on the partitioning data (Tiepolo et al., 2002).

The Huashan and Wenyu plutons both display similar negative Ce and Eu anomalies, although in the Huashan pluton, the δCe is slightly lower, and δEu is slightly higher in the Huashan pluton than in the Wenyu pluton (Figure 9), which is contrary to the results of the previous studies (Liu et al., 2022; Wen et al., 2020; Zhi et al., 2019; Liu et al., 2019). Figure 8F also shows the lack of any obvious correlation between δCe and δEu. King et al. (2013) reported significant (Nb, Ta)$^{4+}$ and/or V^{5+}, the $^{VI}Ce^{3+}/^{VI}Ce^{4+}$ coupled substitutions in Ti-site under oxidizing conditions. Based on the above discussion, we argue that Ce usually substitutes in the Ca-site in the form of Ce^{3+} like other common REE^{3+}; however, even if Ce^{3+} is oxidized to Ce^{4+}, it can still enter into the titanite structure. The good correlation in Figures 8D, E shows substitution in titanite within these rocks. The lack of correlation, as shown in Figure 8F, and higher δCe of the Wenyu pluton compared to the Huashan pluton may also suggest that the δCe of titanite may not always indicate fo_2 of coexisting melts.

The positive Eu anomalies (Figure 9B) might not be well-correlated with fo_2 accelerated by metasomatism (Lottermoser, 1992; Micko, 2010) or short-term elevated temperature (Mazdab et al., 2007). In addition, the titanite from the Huashan pluton shows highly variable δEu than that from

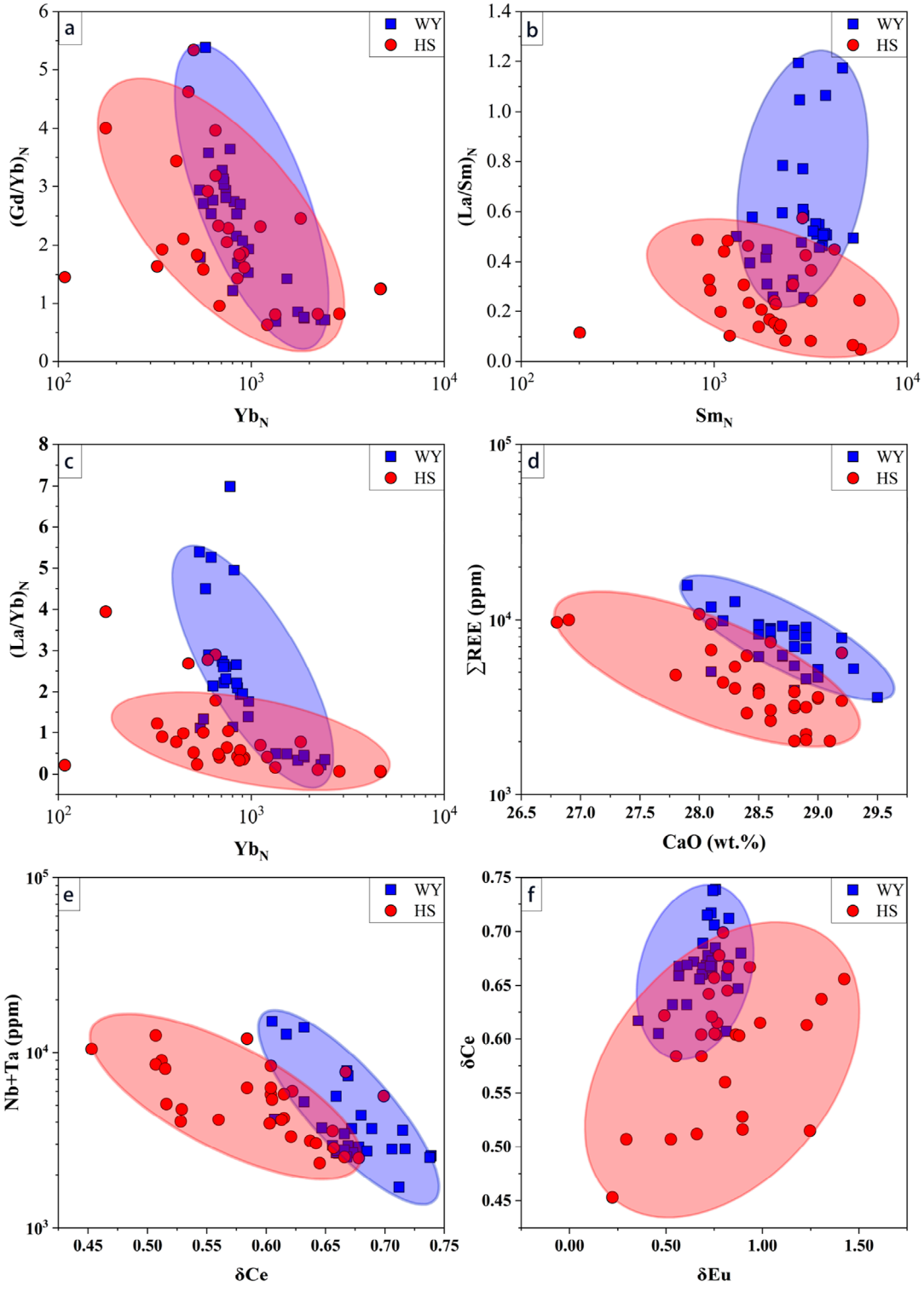

FIGURE 8
Binary plots of the titanite grains from the Huashan and Wenyu plutons: **(A)** $(Gd/Yb)_N$ ratios vs. Yb_N; **(B)** $(La/Sm)_N$ ratios vs. Sm_N; **(C)** $(La/Yb)_N$ ratios vs. Yb_N; **(D)** ΣREE vs. CaO; **(E)** (Nb+Ta) vs. δCe; **(F)** δCe vs. δEu. Normalizing values taken from Boynton (1984) (Zhang, 2015).

Wenyu (Figures 9A, B). Eu is enriched in plagioclase, and minor plagioclase crystallization causes Eu-depletion in melts (Ismail et al., 2014; Ballard et al., 2002; Anand and Balakrishnan, 2011; Bi et al., 2002; Buick et al., 2010). Therefore, the lower δEu might have been largely caused by plagioclase crystallization.

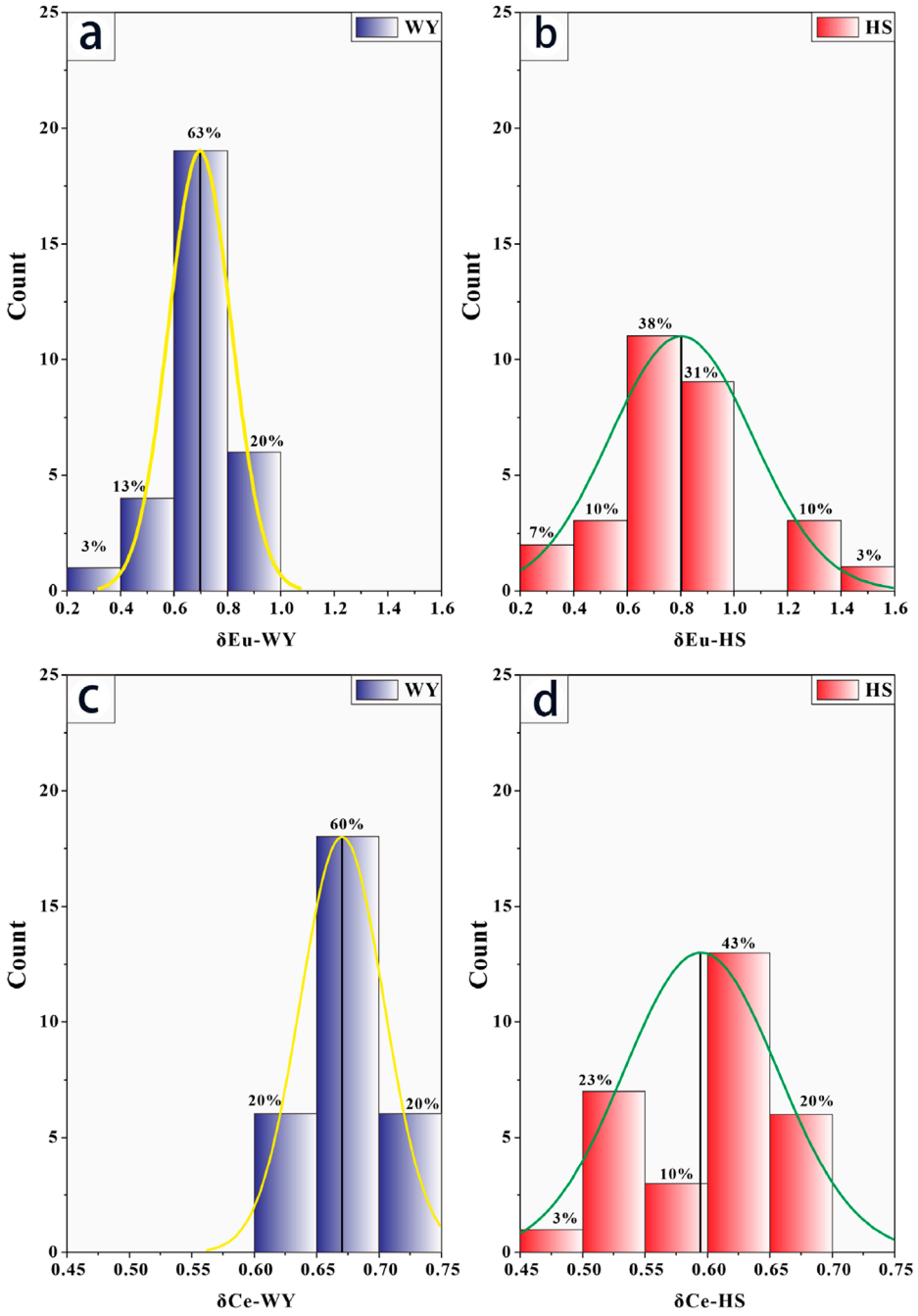

FIGURE 9
Statistical plot of δCe and δEu values of the titanite grains from the Huashan and Wenyu plutons. **(A)** Wenyu titanite δEu values histogram; **(B)** Huashan titanite δEu values histogram; **(C)** Wenyu titanite δCe values histogram; **(D)** Huashan titanite δCe values histogram.

6.2.2 Vanadium

Oxygen fugacity controls multivalent elements in planetary materials and their distribution between phases, which can be used as a proxy for fo_2 (Holycross and Cottrell, 2020). The abundance of V can be exploited as a proxy for fo_2 when its partitioning behavior is known (Holycross and Cottrell, 2020). Vanadium oxygen barometers have been experimentally calibrated for a wide variety of mineral-melt systems to investigate how V partitioning shifts as a function of fo_2 (Arató and Audétat, 2017; Canil, 1997; Canil, 2002; Canil and Fedortchouk, 2000; Canil and Fedortchouk, 2001; Laubier et al., 2014; Mallmann and O'Neill, 2009; Shishkina et al., 2018; Sossi et al., 2018; Toplis and Corgne, 2002; Wang et al., 2019). The whole-rock trace elements result shows that the vanadium concentration in the Wenyu pluton (27.30 ppm) is significantly higher than that in the Huashan pluton (15.40 ppm), and compared with the Huashan pluton, the Wenyu pluton was formed in a relatively high oxygen fugacity environment (Qing and Han, 2001). We found similar results from the titanite component in our

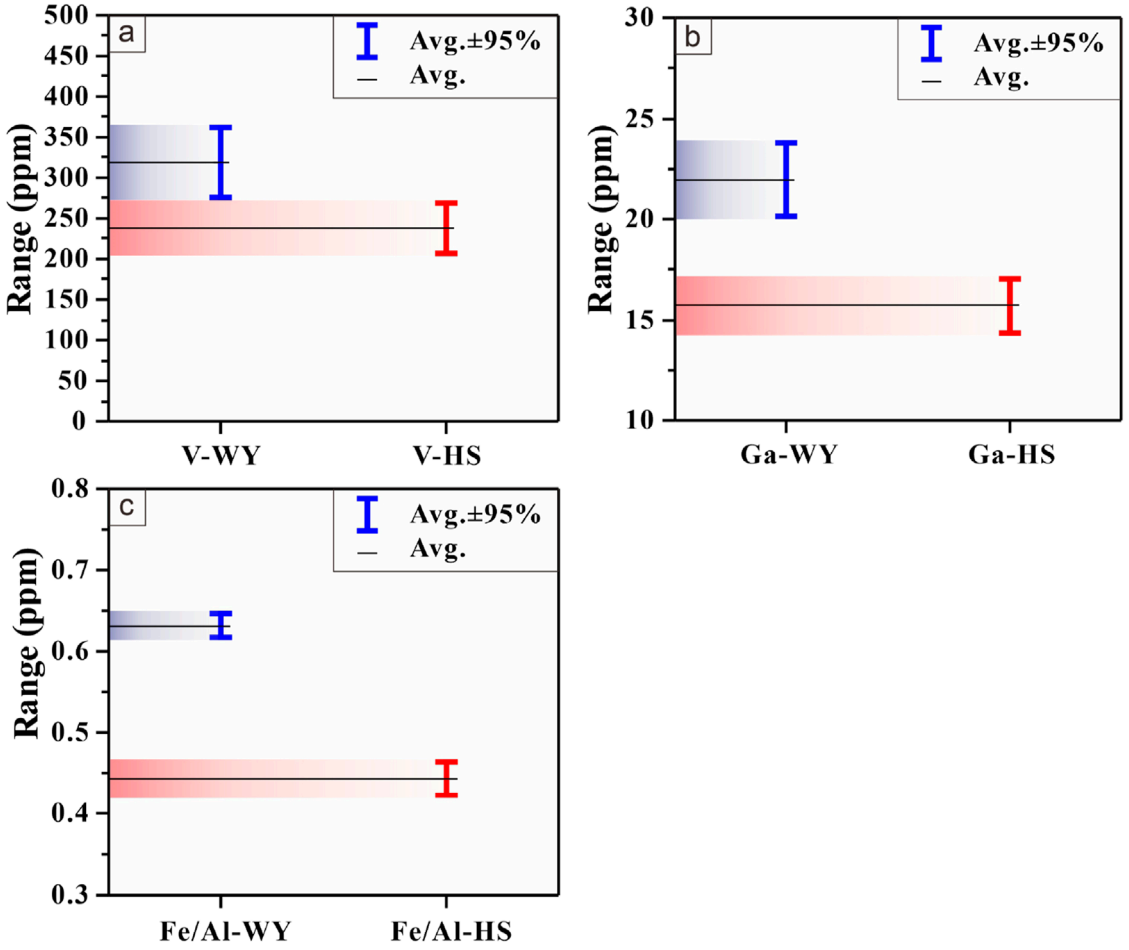

FIGURE 10
Vanadium and gallium concentration and the Fe/Al ratio comparison diagram of the titanite grains from the Huashan and Wenyu pluton. **(A)** Titanite vanadium concentration comparison diagram; **(B)** Titanite gallium concentration comparison diagram; **(C)** Titanite Fe/Al ratio comparison diagram.

research. There is a noticeable difference in the content of V in the titanite samples from the Huashan pluton (74.22–342.09 ppm, Avg. 237.66 ppm) and the Wenyu (51.65–724.85 ppm, Avg. 318.55 ppm) pluton. Figure 10A shows that the fo_2 of the Wenyu pluton is higher than that of the Huashan pluton, as measured by the vanadium content. Bernau and Franz (1987) reported that the possible valence states of vanadium are V^{3+}, V^{4+}, and V^{5+}, but the major substitutions for vanadium occur by the following reaction:

$$2Ti^{4+} = V^{5+} + (Al, Fe)^{3+}.$$

Vanadium is probably pentavalent in titanite because of the high oxidation state of the mineral. Micko (2010) proposed that under high fo_2 oxidizing conditions, V is more soluble and mobile. Therefore, we considered that titanite could be a sink for V^{5+} and the vanadium content in titanite might be a measurement of fo_2 the pluton.

6.2.3 Gallium

Ga^{3+}, Fe^{3+}, and Al^{3+} exhibit similar geochemical characteristics (Breiter et al., 2013; Luo et al., 2007; Macdonald et al., 2010; Tu et al., 2004). The radius of $^{IV}Ga^{3+}$ is comparatively equal to that of $^{IV}Ti^{4+}$ as compared to $^{IV}Fe^{3+}$ and $^{IV}Al^{3+}$ (Shannon, 1976). Xu et al. (2015) reported that Ga^{3+} enters the Ti-site more readily than Al^{3+} and Fe^{3+}, and magmatic fo_2 could be measured by the Ga content in titanite because of the positive correlation between fo_2 and Ga content. A higher Ga content indicates a higher oxidizing environment (Pan et al., 2018). The Ga content in titanite of the Wenyu pluton is distinctively higher (14.46–38.21 ppm, Avg. 21.94 ppm) than that of the Huashan pluton (9.89–22.64 ppm, Avg. 15.71 ppm), which indicates higher fo_2 for the Wenyu pluton (Figure 10B).

6.2.4 Fe/Al ratios

In titanite, the Ti-site is normally occupied by Ti^{4+}, but the commonly substituting cations are Fe^{3+} and Al^{3+} (Deer et al., 2013). Kowallis et al. (1997) reported that high fo_2 will cause the oxidation of Fe^{2+} to Fe^{3+}. Based on the whole-rock major elements, Qing and Han (2001) found that the Wenyu pluton shows relatively higher Fe^{3+} proportion and lower A/CNK ratio than the Huashan pluton. As discussed in Section 5.1, the titanite from the Wenyu pluton shows an Fe/Al ratio ranging from 0.5 to 1 than that of the Huashan pluton (Figure 10C). Therefore, we considered that the

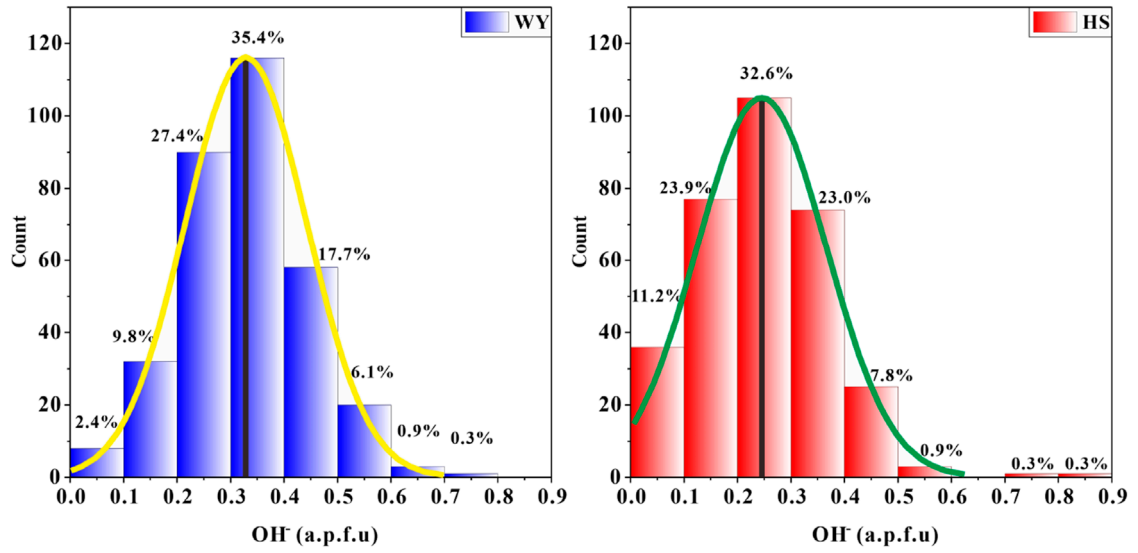

FIGURE 11
Histogram of the hydroxyl ion concentration in the titanite grains from the Huashan and Wenyu plutons.

titanite Fe/Al ratio is also a key parameter for measuring fo_2 of plutons and that the fo_2 of the Wenyu pluton is higher than that of the Huashan pluton.

6.3 Comparison of the relative water content

The OH^- concentration in each mineral species is variable; therefore, in some cases, it reflects the geological environment of mineral formation (Bell David and Rossman George, 1992). Titanite is an essential anhydrous mineral phase in igneous rocks, and the OH^- concentration in titanite may reflect fluctuations in the composition of the magmatic system during the formation of titanite (Hammer et al., 1996). We calculated the value of OH^- in our titanite samples from the EPMA data based on the work of Oberti et al. (1991). As a water constituent, the hydroxyl ion in titanite might reflect the water content in the pluton. Figure 11 clearly shows that the water content of titanite from the Wenyu pluton is higher than that of titanite from the Huashan pluton, which may reflect the fluid composition differences of the magmatic melt during the formation of titanite.

6.4 Implications for the source of ore-forming materials

Previous studies show that the formation temperature of the Wenyu pluton is higher than that of the Huashan pluton, and both of these two plutons' formation temperatures are over 873.15 K (Liu et al., 2022; Wen et al., 2020; Liu et al., 2019). Higher formation temperature might imply more heat input (Qi, 2010). According to Luan et al. (1985), in the Xiaoqinling gold metallogenic area, the Cl concentration is much higher than that of F, and Au was transported with some complex species in the ore-forming fluids. In the ore-forming magmatic hydrothermal fluids of high fo_2 and temperature over 623.15 K, gold is usually transported as $AuCl^{2-}$, and high fo_2 and water contribution improved the solubility of $AuCl^{2-}$ and the amount of solute (Au) in the hydrothermal fluid (An and Zhu, 2011; Castaing et al., 1993; Gammons and Williams-Jones, 1995; Gammons et al., 1997; Gibert et al., 1998; Zhang, 2015; Zhu and An, 2010). Previous studies have shown that many large and medium-sized deposits formed near the Wenyu pluton in the Xiaoqinling area are closely related to fluid activities (Xu et al., 1997; Luan et al., 1985; Jiang, 2000; Wang et al., 2002; Xu et al., 1998; Yang et al., 2015; Yin et al., 2019). The relatively abundant magmatic hydrothermal fluids and higher fo_2 might have led to the Wenyu pluton being more conducive to gold migration, enrichment, and mineralization than the Huashan pluton. In addition, the Wenyu pluton might have experienced a more complex magmatic history than the Huashan pluton, involving more heat input.

7 Conclusion

(1) Titanite from the Wenyu pluton indicates a complex magmatic evolution history, more widespread hydrothermal alteration, and higher silica activity in the melt than in the Huashan pluton.
(2) The substitution mechanism of V and Ga as well as the Fe/Al ratio in titanite indicates that the magma of the Wenyu pluton had higher fo_2 than that of the Huashan pluton.
(3) The water content and fo_2 of the Wenyu plutonic magma were higher than those of the Huashan magma, which imply that the Wenyu plutonic magma was more conducive to gold migration, enrichment, and mineralization than the Huashan plutonic magma.

Data availability statement

The original contributions presented in the study are included in the article/Supplementary Material; further inquiries can be directed to the corresponding author.

Author contributions

QW: conceptualization, formal analysis, investigation, methodology, visualization, writing–original draft, and writing–review and editing. LL: conceptualization, resources, supervision, and writing–review and editing. S-RL: conceptualization, resources, supervision, and writing–review and editing. MS: investigation and writing–review and editing. MA: investigation and writing–review and editing. Z-YC: investigation, resources, validation, and writing–review and editing. M-GL: investigation and writing–review and editing. X-DC: resources, validation, and writing–review and editing. Z-HW: investigation and writing–review and editing. J-WL: investigation and writing–review and editing.

Funding

The author(s) declare that financial support was received for the research, authorship, and/or publication of this article. This study was funded by grants from the Ministry of Science and Technology of the People's Republic of China (2016YFC0600106) to Prof. Lin Li and from the Fundamental Research Funds for the Central Universities (2652017248) to Prof. Sheng-Rong Li.

Acknowledgments

We are grateful to associate editor Prof. Yong Wang, and two reviewers, Prof. Xiao-Dong Deng and Prof. Wei Wang, for their constructive comments which greatly improved the quality of our manuscript.

Conflict of interest

The authors declare that the research was conducted in the absence of any commercial or financial relationships that could be construed as a potential conflict of interest.

Publisher's note

Supplementary material

The Supplementary Material for this article can be found online at: https://www.frontiersin.org/articles/10.3389/feart.2024.1487176/full#supplementary-material

References

Aleksandrov, S. M., and Troneva, M. A. (2007). Composition, mineral assemblages, and genesis of titanite and malayaite in skarns. *Geochem. Int.* 45, 1012–1024. doi:10.1134/S0016702907100059

An, F., and Zhu, Y. F. (2011). Geochemistry of hydrothermal gold mineralization. *Mineral. Deposits* 30, 799–814. doi:10.3969/j.issn.0258-7106.2011.05.004

Anand, R., and Balakrishnan, S. (2011). Geochemical and Sm–Nd isotopic study of titanite from granitoid rocks of the eastern Dharwar craton, southern India. *J. Earth Syst. Sci.* 120, 237–251. doi:10.1007/s12040-011-0045-x

Arató, R., and Audétat, A. (2017). Experimental calibration of a new oxybarometer for silicic magmas based on vanadium partitioning between magnetite and silicate melt. *Geochimica Cosmochimica Acta* 209, 284–295. doi:10.1016/j.gca.2017.04.020

Ballard, J. R., Palin, M. J., and Campbell, I. H. (2002). Relative oxidation states of magmas inferred from Ce(IV)/Ce(III) in zircon: application to porphyry copper deposits of northern Chile. *Contributions Mineralogy Petrology* 144, 347–364. doi:10.1007/s00410-002-0402-5

Bell David, R., and Rossman George, R. (1992). Water in earth's mantle: the role of nominally anhydrous minerals. *Science* 255, 1391–1397. doi:10.1126/science.255.5050.1391

Bernau, R., and Franz, G. (1987). Crystal chemistry and genesis of Nb-, V-, and Al-rich metamorphic titanite from Egypt and Greece. *Can. Mineralogist* 25, 695–705. Available at: https://pubs.geoscienceworld.org/mac/canmin/article-abstract/25/4/695/11994/Crystal-chemistry-and-genesis-of-Nb-V-and-Al-rich?redirectedFrom=PDF.

Bi, X. W., Cornell, D. H., and Hu, R. Z. (2002). REE composition of primary and altered feldspar from the mineralized alteration zone of alkaline intrusive rocks, western Yunnan Province, China. *Ore Geol. Rev.* 19, 69–78. doi:10.1016/S0169-1368(01)00034-8

Breiter, K., Gardenová, N., Kanický, V., and Vaculovič, T. (2013). Gallium and germanium geochemistry during magmatic fractionation and post-magmatic alteration in different types of granitoids: a case study from the Bohemian Massif (Czech Republic). *Geol. Carpathica* 64, 171–180. doi:10.2478/geoca-2013-0018

Buick, L. S., Clark, C., Rubatto, D., Hermann, J., Pandit, M., and Hand, M. (2010). Constraints on the Proterozoic evolution of the Aravalli–Delhi Orogenic belt (NW India) from monazite geochronology and mineral trace element geochemistry. *Lithos* 120, 511–528. doi:10.1016/j.lithos.2010.09.011

Buick, L. S., Hermann, J., Maas, R., and Gibson, R. L. (2007). The timing of sub-solidus hydrothermal alteration in the Central Zone, Limpopo Belt (South Africa): constraints from titanite U–Pb geochronology and REE partitioning. *Lithos* 98, 97–117. doi:10.1016/j.lithos.2007.02.002

Canil, D. (1997). Vanadium partitioning and the oxidation state of Archaean komatiite magmas. *Nature* 389, 842–845. doi:10.1038/39860

Canil, D. (2002). Vanadium in peridotites, mantle redox and tectonic environments: archean to present. *Earth Planet. Sci. Lett.* 195, 75–90. doi:10.1016/S0012-821X(01)00582-9

Canil, D., and Fedortchouk, Y. (2000). Clinopyroxene-liquid partitioning for vanadium and the oxygen fugacity during formation of cratonic and oceanic mantle lithosphere. *J. Geophys. Res. Solid Earth* 105, 26003–26016. doi:10.1029/2000JB900221

Canil, D., and Fedortchouk, Y. (2001). Olivine-liquid partitioning of vanadium and other trace elements, with applications to modern and ancient picrites. *Can. Mineralogist* 39, 319–330. doi:10.2113/gscanmin.39.2.319

Castaing, C., Cassard, D., Gros, Y., Moisy, M., and Chabod, J. C. (1993). Role of rheological heterogeneities in vein-ore localization. *Can. J. Earth Sci.* 30, 113–123. doi:10.1139/e93-011

Che, X. D., Linnen, R. L., Wang, R. C., Groat, L. A., and Brand, A. A. (2013). Distribution of trace and rare earth elements in titanite from tungsten and molybdenum deposits in Yukon and British Columbia, Canada. *Can. Mineralogist* 51, 415–438. doi:10.3749/canmin.51.3.415

Chen, L. (2006). "Characteristics of ore-forming fluid and ore genesis of Dahu gold deposit," in *Xiaoqinling gold area* Beijing: China university of Geosciences).

Chen, X. L., Liang, H. Y., Zhang, J., Sotiriou, P., Huang, W. T., Ren, L., et al. (2019). Geochemical characteristics and magma fertility for the Jurassic arc rocks in the Gangdese belt, Tibet. *Ore Geol. Rev.* 115, 103169. doi:10.1016/j.oregeorev.2019.103169

Cherniak, D. J. (2006). Zr diffusion in titanite. *Contributions Mineralogy Petrology* 152, 639–647. doi:10.1007/s00410-006-0133-0

Chiaradia, M., Schaltegger, U., Spikings, R., Wotzlaw, J.-F., and Ovtcharova, M. (2013). How accurately can we date the duration of magmatic-hydrothermal events in porphyry systems? an invited paper. *Econ. Geol.* 108, 565–584. doi:10.2113/econgeo.108.4.565

Deer, W. A., Howie, R. A., and Zussman, J. (2013). *An introduction to the rock-forming minerals*. Third edition. London: The Mineralogical Society, 15–16.

Deng, X. Q., Zhao, T. P., and Peng, T. P. (2016). Age and geochemistry of the early Mesoproterozoic A-type granites in the southern margin of the North China Craton: constraints on their petrogenesis and tectonic implications. *Precambrian Res.* 283, 68–88. doi:10.1016/j.precamres.2016.07.018

Dong, Y. P., and Santosh, M. (2016). Tectonic architecture and multiple orogeny of the qinling orogenic belt, Central China. *Gondwana Res.* 29, 1–40. doi:10.1016/j.gr.2015.06.009

Dong, Y. P., Sun, S. S., Santosh, M., Zhao, J., Sun, J. P., He, D. F., et al. (2021). Central China orogenic belt and amalgamation of east asian continents. *Gondwana Res.* 100, 131–194. doi:10.1016/j.gr.2021.03.006

Dong, Y. P., Zhang, G. W., Neubauer, F., Liu, X. M., Genser, J., and Hauzenberger, C. (2011). Tectonic evolution of the Qinling orogen, China: review and synthesis. *J. Asian Earth Sci.* 41, 213–237. doi:10.1016/j.jseaes.2011.03.002

Fan, H. R., Xie, Y. H., Zhao, R., and Wang, Y. L. (2000). Dual origins of Xiaoqinling gold-bearing quartz veins:Fluid inclusion evidence. *Chin. Sci. Bull.* 45, 1424–1430. doi:10.1007/BF02886252

Feng, J. Z., Yue, Z. S., Xiao, R. G., Sun, W. Z., Wang, X. C., Yan, J. S., et al. (2009). *Metallogenic regularity and prediction of deep gold deposit in Xiaoqinling area*. Beijing: Geological Publishing House, 266.

Frost, B. R., Chamberlain, K. R., and Schumacher, J. C. (2001). Sphene (titanite): phase relations and role as a geochronometer. *Chem. Geol.* 172, 131–148. doi:10.1016/S0009-2541(00)00240-0

Gammons, C. H., and Williams-Jones, A. E. (1995). The solubility of Au-Ag alloy + AgCl in HCl/NaCl solutions at 300°C: new data on the stability of Au (I) chloride complexes in hydrothermal fluids. *Geochimica Cosmochimica Acta* 59, 3453–3468. doi:10.1016/0016-7037(95)00234-Q

Gammons, C. H., Yu, Y. M., and Williams-Jones, A. E. (1997). The disproportionation of gold(I) chloride complexes at 25 to 200°C. *Geochimica Cosmochimica Acta* 61, 1971–1983. doi:10.1016/S0016-7037(97)00060-4

Gibert, F., Pascal, M. L., and Pichavant, M. (1998). Gold solubility and speciation in hydrothermal solutions: experimental study of the stability of hydrosulphide complex of gold (AuHS°) at 350 to 450°C and 500 bars. *Geochimica Cosmochimica Acta* 62, 2931–2947. doi:10.1016/S0016-7037(98)00209-9

Gribble, C. D., and Hall, A. J. (1993). *Optical mineralogy: principles and practice*. New York: Chapman and Hall, 124–125.

Gromet, L. P., and Silver, L. T. (1983). Rare earth element distributions among minerals in a granodiorite and their petrogenetic implications. *Geochimica Cosmochimica Acta* 47, 925–939. doi:10.1016/0016-7037(83)90158-8

Grondahl, C., and Zajacz, Z. (2022). Sulfur and chlorine budgets control the ore fertility of arc magmas. *Nat. Commun.* 13, 4218. doi:10.1038/s41467-022-31894-0

Guo, B., Zhu, L.-M., Li, B., Gong, H.-J., and Wang, J.-Q. (2009). Zircon U-Pb age and Hf isotope composition of the Huashan and Heyu granite plutons at the southern margin of North China Craton: implications for geodynamic setting. *Acta Petrol. Sin. -25*, 265–281. Available at: http://www.ysxb.ac.cn/en/article/id/aps_20090203

Hammer, V. M. F., Beran, A., Endisch, D., and Rauch, F. (1996). OH concentrations in natural titanites determined by FTIR spectroscopy and nuclear reaction analysis. *Eur. J. Mineralogy* 8, 281–288. doi:10.1127/ejm/8/2/0281

Hayden, L. A., Watson, E. B., and Wark, D. A. (2008). A thermobarometer for sphene (titanite). *Contributions Mineralogy Petrology* 155, 529–540. doi:10.1007/s00410-007-0256-y

Holder, R. M., Hacker, B. R., Seward, G. G. E., and Kylander-Clark, A. R. C. (2019). Interpreting titanite U–Pb dates and Zr thermobarometry in high-grade rocks: empirical constraints on elemental diffusivities of Pb, Al, Fe, Zr, Nb, and Ce. *Contributions Mineralogy Petrology* 174, 42. doi:10.1007/s00410-019-1578-2

Holycross, M., and Cottrell, E. (2020). Partitioning of V and 19 other trace elements between rutile and silicate melt as a function of oxygen fugacity and melt composition: implications for subduction zones. *Am. Mineralogist* 105, 244–254. doi:10.2138/am-2020-7013

Hu, Z. C., Zhang, W., Liu, Y. S., Gao, S., Li, M., Zong, K. Q., et al. (2015). Wave signal-smoothing and mercury-removing device for laser ablation quadrupole and multiple collector ICPMS analysis: application to lead isotope analysis. *Anal. Chem.* 87, 1152–1157. doi:10.1021/ac503749k

Ismail, R., Ciobanu, C. L., Cook, N. J., Teale, G. S., Giles, D., Mumm, A. S., et al. (2014). Rare earths and other trace elements in minerals from skarn assemblages, Hillside iron oxide–copper–gold deposit, Yorke Peninsula, South Australia. *Lithos* 184-187, 456–477. doi:10.1016/j.lithos.2013.07.023

Jian, W. (2010). *Geology, fluid inclusion, stable isotope and molybdenite Re–Os age constraints on the genesis of the Dahu Au–Mo deposit, Xiaoqinling region, China*. Beijing), Beijing: China university of Geosciences.

Jiang, N. (2000). Hydrothermal fluid evolution associated with gold mineralization at the Wenyu mine, xiaoqinling district, China. *Resour. Geol.* 50, 103–112. doi:10.1111/j.1751-3928.2000.tb00060.x

King, P. L., Sham, T.-K., Gordon, R. A., and Dyar, M. D. (2013). Microbeam X-ray analysis of Ce3+/Ce4+ in Ti-rich minerals: a case study with titanite (sphene) with implications for multivalent trace element substitution in minerals. *Am. Mineralogist* 98, 110–119. doi:10.2138/am.2013.3959

Klein, C., and Dutrow, B. (2007). *The 23rd edition of the manual of mineral science: (after James D. Dana)*. 23rd ed. Hoboken, N.J: John Wiley and Sons, Inc., 496–497.

Kohn, M. J. (2017). Titanite petrochronology. *Rev. Mineralogy Geochem.* 83, 419–441. doi:10.2138/rmg.2017.83.13

Kontonikas-Charos, A., Ehrig, K., Cook, N. J., and Ciobanu, C. L. (2019). Crystal chemistry of titanite from the Roxby Downs Granite, South Australia: insights into petrogenesis, subsolidus evolution and hydrothermal alteration. *Contributions Mineralogy Petrology* 174, 59. doi:10.1007/s00410-019-1594-2

Kowallis, B. J., Christiansen, E. H., Dorais, M. J., Winkel, A., Henze, P., Franzen, L., et al. (2018). Compositional variation of Fe, Al and F in titanite (sphene). *Proc. GSA 2018 Annu. Meet. Indianap. Indiana, U. S. A. Monday* 1, 30. Available at: https://www.academia.edu/120585557/Compositional_Variation_of_Fe_Al_and_F_in_Titanite_Sphene_

Kowallis, B. J., Christiansen, E. H., and Griffen, D. T. (1997). "Compositional variations in titanite," in *Proceedings of the geological society of America abstracts with programs*, A–402. Available at: https://www.academia.edu/1454390/Compositional_variations_in_titanite?sm=b

Laubier, M., Grove, T. L., and Langmuir, C. H. (2014). Trace element mineral/melt partitioning for basaltic and basaltic andesitic melts: an experimental and laser ICP-MS study with application to the oxidation state of mantle source regions. *Earth Planet. Sci. Lett.* 392, 265–278. doi:10.1016/j.epsl.2014.01.053

Li, J.-W., Bi, S.-J., Selby, D., Chen, L., Vasconcelos, P., Thiede, D., et al. (2012b). Giant Mesozoic gold provinces related to the destruction of the North China craton. *Earth Planet. Sci. Lett.* 349-350, 26–37. doi:10.1016/j.epsl.2012.06.058

Li, J.-W., Li, Z. K., Zhou, M. F., Chen, L., Bi, S. J., Deng, X. D., et al. (2012a). The early cretaceous Yangzhaiyu lode gold deposit, north China craton: a link between craton reactivation and gold veining. *Econ. Geol.* 107, 43–79. doi:10.2113/econgeo.107.1.43

Li, L., Li, C., Li, Q., Yuan, M. W., Zhang, J. Q., Li, S. R., et al. (2022). Indicators of decratonic gold mineralization in the North China Craton. *Earth-Science Rev.* 228, 103995. doi:10.1016/j.earscirev.2022.103995

Li, L., Li, S. R., Santosh, M., Li, Q., Gu, Y., Lü, W. J., et al. (2016). Dyke swarms and their role in the genesis of world-class gold deposits: insights from the Jiaodong peninsula, China. *J. Asian Earth Sci.* 130, 2–22. doi:10.1016/j.jseaes.2016.06.015

Li, L., Santosh, M., and Li, S. R. (2015). The 'Jiaodong type' gold deposits: characteristics, origin and prospecting. *Ore Geol. Rev.* 65, 589–611. doi:10.1016/j.oregeorev.2014.06.021

Li, S. M., Qu, L. Q., Su, Z. B., Huang, J. J., Wang, X. S., and Yue, Z. S. (1996). *The geology and metallogenic prediction of the gold deposit in Xiaoqinling (in Chinese)*. Beijing: Geological Publishing House.

Li, S. R., and Santosh, M. (2014). Metallogeny and craton destruction: records from the North China craton. *Ore Geol. Rev.* 56, 376–414. doi:10.1016/j.oregeorev.2013.03.002

Li, S. R., and Santosh, M. (2017). Geodynamics of heterogeneous gold mineralization in the North China Craton and its relationship to lithospheric destruction. *Gondwana Res.* 50, 267–292. doi:10.1016/j.gr.2017.05.007

Li, S. R., Santosh, M., Zhang, H. F., Luo, J. Y., Zhang, J. Q., Li, C. L., et al. (2014). Metallogeny in response to lithospheric thinning and craton destruction: geochemistry and U–Pb zircon chronology of the Yixingzhai gold deposit, central North China Craton. *Ore Geol. Rev.* 56, 457–471. doi:10.1016/j.oregeorev.2012.10.008

Li, S. R., Santosh, M., Zhang, H. F., Shen, J. F., Dong, G. C., Wang, J. Z., et al. (2013). Inhomogeneous lithospheric thinning in the central North China Craton: zircon U–Pb and S–He–Ar isotopic record from magmatism and metallogeny in the Taihang Mountains. *Gondwana Res.* 23, 141–160. doi:10.1016/j.gr.2012.02.006

Liu, J. W., Li, L., Li, S. R., Santosh, M., and Yuan, M. W. (2022). Apatite as a fingerprint of granite fertility and gold mineralization: evidence from the xiaoqinling goldfield, north China craton. *Ore Geol. Rev.* 142, 104720. doi:10.1016/j.oregeorev.2022.104720

Liu, J. W., Li, S. R., Yuan, M. W., Li, S. S., Zhi, Z. Y., and Wen, Z. H. (2019). Apatite-zircon constraints on the magmatic oxygen fugacity for the granitic plutons in the Xiaoqinling gold province. *Acta Mineral. Sin.* 39, 494–506. doi:10.16461/j.cnki.1000-4734.2019.39.037

Liu, Y. S., Hu, Z. C., Gao, S., Günther, D., Xu, J., Gao, C. G., et al. (2008). *In situ* analysis of major and trace elements of anhydrous minerals by LA-ICP-MS without applying an internal standard. *Chem. Geol.* 257, 34–43. doi:10.1016/j.chemgeo.2008.08.004

Lottermoser, B. G. (1992). Rare earth elements and hydrothermal ore formation processes. *Ore Geol. Rev.* 7, 25–41. doi:10.1016/0169-1368(92)90017-F

Luan, S. W., Cao, D. C., Fang, Y. K., and Wang, J. Y. (1985). Geochemistry of xiaoqinling gold deposits. *Minerals Rocks*, 1–133. doi:10.19719/j.cnki.1001-6872.1985.02.001

Lucassen, F., Franz, G., Dulski, P., Romer, R. L., and Rhede, D. (2011). Element and Sr isotope signatures of titanite as indicator of variable fluid composition in hydrated eclogite. *Lithos* 121, 12–24. doi:10.1016/j.lithos.2010.09.018

Luo, T. Y., Dai, X. D., Zhu, D., Tao, Y., Song, X. Y., and Zhang, H. (2007). Mineralization of gallium: implications to emeishan large igneous province. *Acta Mineral. Sin.* 27, 281–286. doi:10.3321/j.issn:1000-4734.2007.03.009

Macdonald, R., Rogers, N. W., Bagiński, B., and Dzierżanowski, P. (2010). Distribution of gallium between phenocrysts and melt in peralkaline salic volcanic rocks, Kenya Rift Valley. *Mineral. Mag.* 74, 351–363. doi:10.1180/minmag.2010.074.2.351

Mallmann, G., and O'Neill, H. S. C. (2009). The crystal/melt partitioning of V during mantle melting as a function of oxygen fugacity compared with some other elements (Al, P, Ca, Sc, Ti, Cr, Fe, Ga, Y, Zr and Nb). *J. Petrology* 50, 1765–1794. doi:10.1093/petrology/egp053

Mao, J. W., Goldfarb, R. J., Zhang, Z. W., Xu, W. Y., Qiu, Y. M., and Deng, J. (2002). Gold deposits in the xiaoqinling–xiong'ershan region, qinling mountains, central China. *Miner. Deposita* 37, 306–325. doi:10.1007/s00126-001-0248-1

Mao, J. W., Hua, R. M., and Li, X. B. (1999). A preliminary study of large-scale metallogenesis and large clusters of mineral deposits. *Mineral. Deposits* 18, 291–299. doi:10.3969/j.issn.0258-7106.1999.04.001

Mao, J.-W., Xie, G.-Q., Pirajno, F., Ye, H.-S., Wang, Y.-B., Li, Y.-F., et al. (2010). Late Jurassic–Early Cretaceous granitoid magmatism in Eastern Qinling, central-eastern China: SHRIMP zircon U–Pb ages and tectonic implications. *Aust. J. Earth Sci.* 57, 51–78. doi:10.1080/08120090903416203

Mazdab, F. K., Wooden, J. L., and Barth, A. P. (2007). "Trace element variability in titanite from diverse geologic environments," in Proceedings of the The GSA 2007 Annual Meeting, Denver, Colorado, USA, Tuesday, 30 October 2007, 406. 8:00 AM-12:00 PM.

McLeod, G. W. (2009). *Titanite zoning and magma mixing*. Glasgow, Scotland: University of Glasgow.

McLeod, G. W., Dempster, T. J., and Faithfull, J. W. (2010). Deciphering magma-mixing processes using zoned titanite from the ross of mull granite, scotland. *J. Petrology* 52, 55–82. doi:10.1093/petrology/egq071

Micko, J. (2010). *The geology and genesis of the Central Zone alkalic copper-gold porphyry deposit, Galore Creek district, northwestern*. British Columbia, Canada: University of British Columbia.

Nakada, S. (1991). Magmatic processes in titanite-bearing dacites, central Andes of Chile and Bolivia. *Am. Mineralogist* 76, 548–560. Available at: https://search.library.berkeley.edu/permalink/01UCS_BER/s4lks2/cdi_geoscienceworld_journals_1991_040177.

Nathwani, C. L., Wilkinson, J. J., Fry, G., Armstrong, R. N., Smith, D. J., and Ihlenfeld, C. (2022). Machine learning for geochemical exploration: classifying metallogenic fertility in arc magmas and insights into porphyry copper deposit formation. *Miner. Deposita* 57, 1143–1166. doi:10.1007/s00126-021-01086-9

Oberti, R., Smith, D. C., Rossi, G., and Caucia, F. (1991). The crystal-chemistry of high-aluminium titanites. *Eur. J. Mineralogy* 3, 777–792. doi:10.1127/ejm/3/5/0777

Pan, L. C., Hu, R. Z., Bi, X. W., Li, C. S., Wang, X. S., and Zhu, J. J. (2018). Titanite major and trace element compositions as petrogenetic and metallogenic indicators of Mo ore deposits: examples from four granite plutons in the southern Yidun arc, SW China. *Am. Mineralogist* 103, 1417–1434. doi:10.2138/am-2018-6224

Pan, Y. M., Fleet, M. E., and MacRae, N. D. (1993). Late alteration in titanite (CaTiSiO5): redistribution and remobilization of rare earth elements and implications for U/Pb and Th/Pb geochronology and nuclear waste disposal. *Geochimica Cosmochimica Acta* 57, 355–367. doi:10.1016/0016-7037(93)90437-2

Perkins, D. (2013). *Mineralogy*. 3rd ed. London: Pearson, 413–414.

Piccoli, P., Candela, P., and Rivers, M. (2000). Interpreting magmatic processes from accessory phases: titanite—a small-scale recorder of large-scale processes. *Earth Environ. Sci. Trans. R. Soc. Edinb.* 91, 257–267. doi:10.1017/S0263593300007422

Prowatke, S., and Klemme, S. (2005). Effect of melt composition on the partitioning of trace elements between titanite and silicate melt. *Geochimica Cosmochimica Acta* 69, 695–709. doi:10.1016/j.gca.2004.06.037

Qi, K. J. (2010). *Mineralization law and metallogenic prognosis of the xiaoqinling gold ore field*. Beijing), Beijing: China University of Geosciences.

Qing, M., and Han, X. J. (2001). The auriferous difference and its appraisal criteria for magnetite series granite in the western Henan province. *J. Mineralogy Petrology* 12, 26. doi:10.19719/j.cnki.1001-6872.2001.04.005

Redin, Y. O., Redina, A. A., Mokrushnikov, V. P., Malyutina, A. V., and Dultsev, V. F. (2022). Rock-forming (biotite and plagioclase) and accessory (zircon) minerals geochemistry as an indicator of the metal fertility of magmas by the example of Au-Cu-Fe-skarn deposits in eastern transbaikalia. *Minerals* 12, 50. doi:10.3390/min12010050

Santosh, M., and Groves, D. I. (2022). Global metallogeny in relation to secular evolution of the Earth and supercontinent cycles. *Gondwana Res.* 107, 395–422. doi:10.1016/j.gr.2022.04.007

Shannon, R. D. (1976). Revised effective ionic radii and systematic studies of interatomic distances in halides and chalcogenides. *Acta Crystallogr.* A32, 751–767. doi:10.1107/S0567739476001551

Shishkina, T. A., Portnyagin, M. V., Botcharnikov, R. E., Almeev, R. R., Simonyan, A. V., Garbe-Schönberg, D., et al. (2018). Experimental calibration and implications of olivine-melt vanadium oxybarometry for hydrous basaltic arc magmas. *Am. Mineralogist* 103, 369–383. doi:10.2138/am-2018-6210

Shu, Q. H., Chang, Z. S., Lai, Y., Hu, X. L., Wu, H. Y., Zhang, Y., et al. (2019). Zircon trace elements and magma fertility: insights from porphyry (-skarn) Mo deposits in NE China. *Miner. Deposita* 54, 645–656. doi:10.1007/s00126-019-00867-7

Smith, M. P., Storey, C. D., Jeffries, T. E., and Ryan, C. (2009). *In situ* U–Pb and trace element analysis of accessory minerals in the kiruna district, norrbotten, Sweden: new constraints on the timing and origin of mineralization. *J. Petrology* 50, 2063–2094. doi:10.1093/petrology/egp069

Song, S. W., Mao, J. W., Xie, G. Q., Chen, L., Santosh, M., Chen, G. H., et al. (2019). *In situ* LA-ICP-MS U–Pb geochronology and trace element analysis of hydrothermal titanite from the giant Zhuxi W (Cu) skarn deposit, South China. *Miner. Deposita* 54, 569–590. doi:10.1007/s00126-018-0831-3

Sossi, P. A., Prytulak, J., and O'Neill, H. S. C. (2018). Experimental calibration of vanadium partitioning and stable isotope fractionation between hydrous granitic melt and magnetite at 800 °C and 0.5 GPa. *Contributions Mineralogy Petrology* 173, 27. doi:10.1007/s00410-018-1451-8

Tiepolo, M., Oberti, R., and Vannucci, R. (2002). Trace-element incorporation in titanite: constraints from experimentally determined solid/liquid partition coefficients. *Chem. Geol.* 191, 105–119. doi:10.1016/S0009-2541(02)00151-1

Toplis, M. J., and Corgne, A. (2002). An experimental study of element partitioning between magnetite, clinopyroxene and iron-bearing silicate liquids with particular emphasis on vanadium. *Contributions Mineralogy Petrology* 144, 22–37. doi:10.1007/s00410-002-0382-5

Trail, D., Watson, E. B., and Tailby, N. D. (2011). The oxidation state of Hadean magmas and implications for early Earth's atmosphere. *Nature* 480, 79–82. doi:10.1038/nature10655

Trail, D., Watson, E. B., and Tailby, N. D. (2012). Ce and Eu anomalies in zircon as proxies for the oxidation state of magmas. *Geochimica Cosmochimica Acta* 97, 70–87. doi:10.1016/j.gca.2012.08.032

Tu, G. C., Gao, Z. M., Hu, R. Z., Zhang, Q., Li, C. Y., Zhao, Z. H., et al. (2004). *The geochemistry and ore-forming mechanism of the dispersed elements (in Chinese)*. Beijing: Geological Publishing House.

Wang, J. T., Xiong, X. L., Takahashi, E., Zhang, L., Li, L., and Liu, X. C. (2019). Oxidation state of arc mantle revealed by partitioning of V, Sc, and Ti between mantle minerals and basaltic melts. *J. Geophys. Res. Solid Earth* 124, 4617–4638. doi:10.1029/2018JB016731

Wang, P. F., Feng, F., Chen, S. Y., Yang, S. Q., Xue, Z. Q., Ding, Y., et al. (2022). Isotopic characteristics of deep veins of Yangzhaiyu gold deposit in Xiaoqinling gold ore field and its constraint on the source of ore-forming fluid. *Mineral Resour. Geol.* 36, 120–128. doi:10.19856/j.cnki.issn.1001-5663.2022.01.015

Wang, R. C., Xie, L., Chen, J., Yu, A. P., Wang, L. B., Liu, J. J., et al. (2011). Titanite as an indicator mineral of tin mineralizing potential of granites in the middle nanling range. *Geol. J. China Univ.* 17, 368–380. doi:10.3969/j.issn.1006-7493.2011.03.002

Wang, R. C., Xie, L., Chen, J., Yu, A. P., Wang, L. B., Lu, J. J., et al. (2013). Tin-carrier minerals in metaluminous granites of the western Nanling Range (southern China): constraints on processes of tin mineralization in oxidized granites. *J. Asian Earth Sci.* 74, 361–372. doi:10.1016/j.jseaes.2012.11.029

Wang, T. J., Fan, B. H., Guan, K., Chen, X. B., He, Y. L., Liu, J., et al. (2002). On the genesis of Wenyu gold deposit (in Chinese). *Contributions Geol. Mineral Resour. Res.* 17, 85–91. doi:10.3969/j.issn.1001-1412.2002.02.003

Wang, Y. F., Shao, Y., Jiang, S. Y., Zhang, Z. Z., Hu, J., Xiao, E., et al. (2012). Petrogenesis of indosinian high Ba-Sr granites in laoniushan batholith, shaanxi province and their tectonic implications. *Geol. J. China Univ.* 18, 133–149. doi:10.16108/j.issn1006-7493.2012.01.012

Wang, Y. L., Xie, Y. H., and Fan, H. R. (1994). Fluid inclusion in Xiaoqinling gold field and its significance to gold mineralization. *Acta Petrol. Sin.* 10, 211–217. Available at: http://www.ysxb.ac.cn/article/id/aps_19940222.

Wang, Y.-T., Ye, H.-S., Ye, A.-W., Shuai, Y., Li, Y.-G., and Zhang, C.-Q. (2010). Zircon SHRIMP U-Pb ages and their significances of the Wenyu and Niangniangshan granitic plutons in the Xiaoqinling area, central China. *Chin. J. Geol.* 45, 167–180. Available at: https://en.cnki.com.cn/Article_en/CJFDTOTAL-DZKX201001016.htm

Wen, Z. H., Li, L., Li, S. R., Santosh, M., Alam, M., Yuan, M. W., et al. (2020). Gold-forming potential of the granitic plutons in the Xiaoqinling gold province, southern margin of the North China Craton: perspectives from zircon U–Pb isotopes and geochemistry. *Geol. J.* 55, 5725–5744. doi:10.1002/gj.3619

Wones, D. R. (1989). Significance of the assemblage titanite+magnetite+quartz in granitic rocks. *Am. Mineralogist* 74, 744–749. Available at: https://pubs.geoscienceworld.org/msa/ammin/article-abstract/74/7-8/744/42272/Significance-of-the-assemblage-titanite-magnetite?redirectedFrom=fulltext.

Wu, T. (2019). *Geochemical characteristics and ore genesis of the Yangzhaiyu gold deposit in Xiaoqinling district*. Beijing), Beijing: China University of Geosciences.

Wu, X. G. (2016). Stable isotope geochemistry and ore-forming materials of the Dongtongyu gold deposit in Xiaoqinling area, China. *Northwest. Geol.* 49, 91–98. Available at: https://www.xbdz.net.cn/cn/article/id/20160409.

Wu, Y. B., Zheng, Y. F., Zhao, Z. F., Gong, B., Liu, X. M., and Wu, F. Y. (2006). U–Pb, Hf and O isotope evidence for two episodes of fluid-assisted zircon growth in marble-hosted eclogites from the Dabie orogen. *Geochimica Cosmochimica Acta* 70, 3743–3761. doi:10.1016/j.gca.2006.05.011

Xiao, X., Zhou, T. F., White, N. C., Zhang, L. L., Fan, Y., and Chen, X. F. (2021). Multiple generations of titanites and their geochemical characteristics record the magmatic-hydrothermal processes and timing of the Dongguashan porphyry-skarn Cu-Au system, Tongling district, Eastern China. *Miner. Deposita* 56, 363–380. doi:10.1007/s00126-020-00962-0

Xie, L., Wang, R. C., Chen, J., and Zhu, J. C. (2010). Mineralogical evidence for magmatic and hydrothermal processes in the Qitianling oxidized tin-bearing granite (Hunan, South China): EMP and (MC)-LA-ICPMS investigations of three types of titanite. *Chem. Geol.* 276, 53–68. doi:10.1016/j.chemgeo.2010.05.020

Xie, L., Wang, R. C., Chen, J., Zhu, J. C., Zhang, W. L., Wang, D. Z., et al. (2009). Primary Sn-rich titianite in the Qitianling granite, Hunan Province, southern China: an important type of tin-bearing mineral and its implications for tin exploration. *Chin. Sci. Bull.* 54, 798–805. doi:10.1007/s11434-008-0557-1

Xie, Y. H., Fan, H. R., and Wang, Y. L. (1998). CO_2-H_2O inclusions and their prospecting significance from granites in Xiaoqinling are, Henan Province. *Acta Petrol. Sin.* 14, 542–548. Available at: http://www.ysxb.ac.cn/article/id/aps_19980463.

Xu, L. L., Bi, X. W., Hu, R. Z., Tang, Y. Y., Wang, X. S., and Xu, Y. (2015). LA-ICP-MS mineral chemistry of titanite and the geological implications for exploration of porphyry Cu deposits in the Jinshajiang – red River alkaline igneous belt, SW China. *Mineralogy Petrology* 109, 181–200. doi:10.1007/s00710-014-0359-x

Xu, Q. D., Zhong, Z. Q., Zhou, H. W., and Zhong, G. L. (1997). Natures of granitic magma and it's relation with gold mineralization in Dongchuang gold field, Xiaoqinling (in Chinese). *Gold Geol.* 3, 19–24. Available at: https://qikan.cqvip.com/Qikan/Article/Detail?id=2713194.

Xu, Q. D., Zhong, Z. Q., Zhou, H. W., and Zhong, G. L. (1998). Relationship between gold mineralization and activity of granitic magma in Xiaoqinling area: evidences from typomorphic peculiarities of fluids (in Chinese). *Geotect. Metallogenia* 22, 35–44. doi:10.16539/j.ddgzyckx.1998.01.006

Yang, C. X., and Santosh, M. (2020). Ancient deep roots for Mesozoic world-class gold deposits in the north China craton: an integrated genetic perspective. *Geosci. Front.* 11, 203–214. doi:10.1016/j.gsf.2019.03.002

Yang, Y. F., Fan, W. Y., Luo, M. J., and Shi, H. Z. (2015). Magmatic hydrothermal origin of the Wenyu copper polymetallic deposit, southern Lancangjiang Zone, SW China. *Acta Geol. Sin. Engl. Ed.* 89, 1769–1770. doi:10.1111/1755-6724.12581

Yin, C., Liu, J. J., Carranza, E. J. M., Zhai, D. G., and Guo, Y. C. (2019). Mineralogical constraints on the genesis of the Dahu quartz vein-style Au-Mo deposit, Xiaoqinling gold district, China: implications for phase relationships and physicochemical conditions. *Ore Geol. Rev.* 113, 103107. doi:10.1016/j.oregeorev.2019.103107

Yu, X.-Q., Liu, J.-L., Zhang, D.-H., Zheng, Y., Li, C.-L., Chen, S.-Q., et al. (2013). Uprising period and elevation of the Wenyu granitic pluton in the Xiaoqinling District, Central China. *Chin. Sci. Bull.* 58, 4459–4471. doi:10.1007/s11434-013-5830-2

Zhang, D. H. (2015). *Geochemistry of ore-forming processes (in Chinese)*. Beijing: Geological Publishing House.

Zhang, G. W., Zhang, B. R., Yuan, X. C., and Xiao, Q. H. (2001). *Qinling orogenic belt and continental dynamics (in Chinese)*. Beijing: Science Press.

Zhang, X.-K., Ye, H.-S., Li, Z.-Y., Cao, J., and Wang, X.-Y. (2015). Zircon U-Pb ages, Hf isotopic composition and geochemistry of Dafuyu granitoid poluton from Huashan complex batholith in Xiaoqinling. *Mineral. Deposits* 34, 235–260.doi:10.16111/j.0258-7106.2015.02.003

Zhao, H. X., Frimmel, H. E., Jiang, S. Y., and Dai, B. Z. (2011). LA-ICP-MS trace element analysis of pyrite from the Xiaoqinling gold district, China: implications for ore genesis. *Ore Geol. Rev.* 43, 142–153. doi:10.1016/j.oregeorev.2011.07.006

Zhao, H.-X., Jiang, S.-Y., Frimmel, H. E., Dai, B.-Z., and Ma, L. (2012). Geochemistry, geochronology and Sr–Nd–Hf isotopes of two Mesozoic granitoids in the Xiaoqinling gold district: implication for large-scale lithospheric thinning in the North China Craton. *Chem. Geol.* 294-295, 173–189. doi:10.1016/j.chemgeo.2011.11.030

Zhao, T. P., Meng, L., Gao, X. Y., Jin, C., Wu, Q., and Bao, Z. W. (2018). Late Mesozoic felsic magmatism and Mo-Au-Pb-Zn mineralization in the southern margin of the North China Craton: a review. *J. Asian Earth Sci.* 161, 103–121. doi:10.1016/j.jseaes.2018.04.020

Zhi, Z. Y., Li, L., Li, S. R., Santosh, M., Yuan, M. W., and Alam, M. (2019). Magnetite as an indicator of granite fertility and gold mineralization: a case study from the Xiaoqinling gold province, North China Craton. *Ore Geol. Rev.* 115, 103159. doi:10.1016/j.oregeorev.2019.103159

Zhou, Z. J., Chen, Y. J., Jiang, S. Y., Hu, C. J., Qin, Y., and Zhao, H. X. (2015). Isotope and fluid inclusion geochemistry and genesis of the Qiangma gold deposit, Xiaoqinling gold field, Qinling Orogen, China. *Ore Geol. Rev.* 66, 47–64. doi:10.1016/j.oregeorev.2014.10.020

Zhou, Z. J., Chen, Y. J., Jiang, S. Y., Zhao, H. X., Qin, Y., and Hu, C. J. (2014). Geology, geochemistry and ore genesis of the Wenyu gold deposit, Xiaoqinling gold field, Qinling Orogen, southern margin of North China Craton. *Ore Geol. Rev.* 59, 1–20. doi:10.1016/j.oregeorev.2013.12.001

Zhou, Z. J., Jiang, S. Y., Qin, Y., Zhao, H. X., and Hu, C. J. (2011). Fluid inclusion characteristics and ore genesis of the Wenyu gold deposit, Xiaoqinling gold belt. *Acta Petrol. Sin.* 27, 3787–3799. Available at: http://www.ysxb.ac.cn/article/id/aps_20111222.

Zhu, R. X., Fan, H. R., Li, J. W., Meng, Q. R., Li, S. R., and Zeng, Q. D. (2015). Decratonic gold deposits. *Sci. China Earth Sci.* 58, 1523–1537. doi:10.1007/s11430-015-5139-x

Zhu, R. X., Xu, Y. G., Zhu, G., Zhang, H. F., Xia, Q. K., and Zheng, T. Y. (2012). Destruction of the North China craton. *Sci. China Earth Sci.* 55, 1565–1587. doi:10.1007/s11430-012-4516-y

Zhu, Y. F., and An, F. (2010). Geochemistry of hydrothermal mineralization: taking gold deposit as an example. *Earth Sci. Front.* 17, 45–52. Available at: https://ir.pku.edu.cn/handle/20.500.11897/50080.

Zong, K. Q., Klemd, R., Yuan, Y., He, Z. Y., Guo, J. L., Shi, X. L., et al. (2017). The assembly of Rodinia: the correlation of early Neoproterozoic (ca. 900Ma) high-grade metamorphism and continental arc formation in the southern Beishan Orogen, southern Central Asian Orogenic Belt (CAOB). *Precambrian Res.* 290, 32–48. doi:10.1016/j.precamres.2016.12.010